ASME 434
Atmospheric Dynamics
Department of Physics
NC A&T State University

Prof. Yuh-Lang Lin
ylin@ncat.edu
https://mesolab.ncat.edu

12. Mesoscale convective systems

(Based on Ch. 9, "Mesoscale Dynamics", by Y.-L. Lin 2007)

Chapter 9 Mesoscale convective systems [Lin 2007]

- A *mesoscale convective system* (MCS) is an organized cluster of thunderstorms, which persists at least for several hours and produces a contiguous precipitation area.

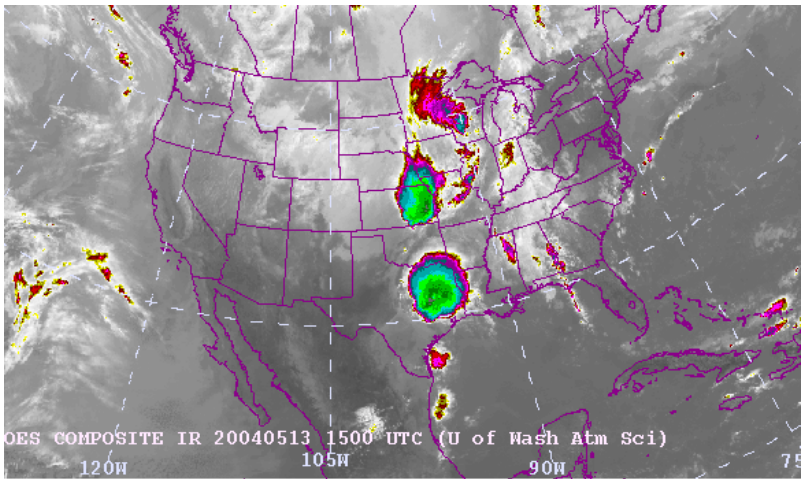

- An MCS may be linear or circular in shape and is often used to refer to a cluster of thunderstorms that does not satisfy the definition of a mesoscale convective complex (MCC) (Section 9.2).

- MCSs include
  - squall lines and MCCs in the midlatitudes, and
  - tropical storms (cyclones) and cloud clusters in the tropics.

- The term *mesoscale convective line* has also been used to represent a linear form of MCSs.

- MCSs have a horizontal scale greater than that of an individual thunderstorm, but smaller than the Rossby radius of deformation.

  Rossby radius of deformation is defined in (4.2.12):

  $L_R = NL_z / f$, where L_z is the vertical scale of the motion.

  In the, $L_R \sim 1000$ km,
  if $N = 0.01$ s^{-1}, $L_z = 10$ km, and $f = 10^{-4}$ s^{-1} (midlat.)

These conditions require the horizontal scale of a MCS to be approximately 100 km.

- Observations have indicated that MCSs have a typical lifetime of 3 hours or more, and their accompanying stratiform clouds sustained for several days.
- Dynamically, this implies that the Coriolis acceleration is at least comparable to the other terms of the momentum equations, such as the inertial acceleration terms. This gives a time scale of f^{-1} (e.g., see Table 1.1), i.e. at least 3 h for midlatitude MCSs, which is consistent with observations.
- In addition to influencing mesoscale weather, MCSs also affect the general circulation.

  This effect occurs due to an energy transfer associated with heating that is comparable in scale to L_R, as discussed in Chapter 1 and revealed in Fig. 1.1.

- MCSs are often composed of ordinary, multicell and/or supercell thunderstorms (the building blocks of the MCS), which exhibit deep, moist convective overturning adjacent to or embedded within a mesoscale vertical circulation that is at least partially driven by convective processes.

- Furthermore, stratiform clouds are often generated and maintained by these MCSs, which may incur heavy stratiform rain, in addition to the heavy rain showers from the convective region (Houze et al. 1989).

- The dynamics of MCSs are rather complicated because in addition to the complicated dynamics of individual, isolated thunderstorms, the interactions among these thunderstorms and the generation and maintenance of the associated stratiform clouds and precipitation have to be considered.

9.1 Squall lines and rainbands

9.1.1 Squall line classifications

- A squall line is an organized line of thunderstorms that produces a contiguous precipitation area.

- The organized convection associated with a squall line is created by deep convective cells on a scale of O(1-10 km), embedded in the mesoscale circulations.

- Based on synoptic environments and flow structures, different conceptual models of squall lines have been proposed (Fig. 9.1):

(a) deep-shear model

(b) shallow-shear model

(c) jet-like shear model

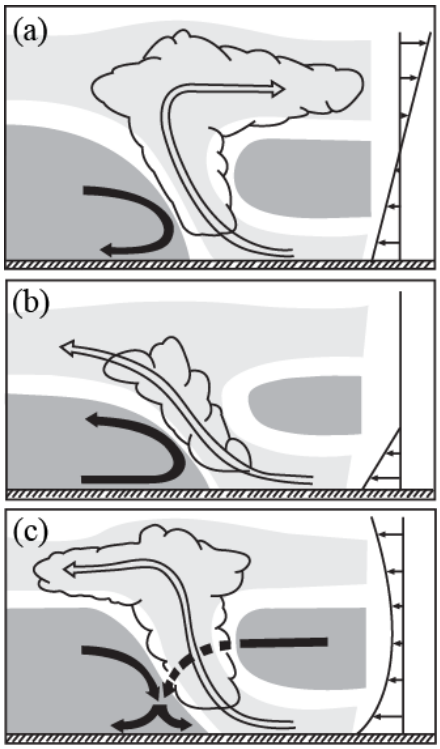

Fig. 9.1: Major conceptual models of squall lines derived from case studies: (a) deep-shear model (Ludlam 1963; Newton 1963); (b) shallow-shear model (Carbone 1982); and (c) jet-like shear model (Zipser 1977). Areas of high (low) θ_e air are lightly (darkly) shaded. [Lin 2007]

These models show that a low-level flow carrying warm, moist, high θ_e air overruns density current-associated low θ_e air.

The lifting of this high θ_e low-level flow by the density current helps raise the low-level air parcels or layer to the realization of conditional or potential instability.

- The deep-shear model (Fig. 9.1a) was the earliest conceptual model with:

  - Deep shear layer, which extends to the middle or upper troposphere.
  - Strong updrafts tend to tilt upshear tilt, which unload its precipitation upshear and permits the updraft and downdraft circulations to continue free of interference.
  - The above occurs only when the cold pool is strong.

  This type of quasi-steady 2D convective cell is the basic building block for a squall line with an upshear tilt that contributes to its longevity by sustaining cool air downdrafts rearward of it.

  Some important dynamics of this type of squall lines are:
  (1) A front-to-rear mid-tropospheric inflow jet develops.
  (2) This midtroposphere jet decreases (increases) the lower (upper)-tropospheric wind shear.
  (3) The mesoscale quasi-stable flow field feeds back into the transient accelerations.
  (4) The upshear tilt of the updraft in most mature squall lines.

➢ A squall line may be composed by a line of rotating supercell storms in a deep, strongly sheared environment (Fig. 9.2).

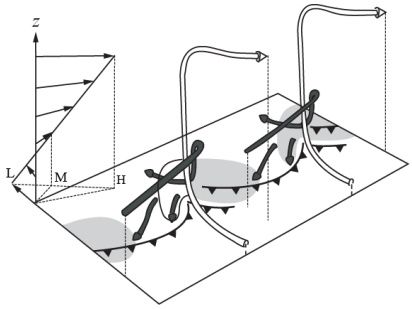

Fig. 9.2: Maintenance of a squall line by three-dimensional effect. See text for detailed description of the mechanism. Streamlines depict flow

relative to the individual supercells. The environmental wind profile is shown on the left. The relative winds at low, middle, and high levels are denoted by L, M, and H, respectively. The shaded regions indicate the radar image hook echo formed by the rain areas and the barbed lines denote the gust fronts. (After Rotunno et al. 1988, based on Lilly 1979) [Lin 2007]

- A squall line may also be composed of multicell storms.

The flow structure is similar to that of the deep-shear model (Fig. 9.1a), except that the air coming from the front of the squall line also feeds the downdraft in the rear part of the storm.

- Unlike the deep-sheared squall lines, many squall lines form in an environment with shallow shear.

  In this type of squall line, the shear is focused in the layer comparable to that of the cold pool. For example, Fig. 9.1b shows a conceptual model of these squall lines, based on an analysis of a California squall line.

- A third type of squall line possesses jet-like shear, but with no steering (critical) levels (Fig. 9.1c).

  During the mature stage of this type of squall lines, there is front-to-rear flow at all levels. In other words, the squall line moves so rapidly (~10 – 15 ms^{-1}) that there exists no critical level in the moving frame of reference.

  Both tropical and midlatitude squall lines of this type share similar flow structures, such as that: (1) both are formed by a line of multicells or supercells and (2) both have pronounced front-to-rear flow that rises at the squall line gust front.

- Mesoscale convective lines may also be classified by their precipitation characteristics and associated flow structures with (Parker and Johnson 2000):
  - (a) *trailing stratiform precipitation* (TS) [~60%]
  - (b) *leading stratiform precipitation* (LS) [~20%]
  - (c) *parallel stratiform precipitation* (PS) [~20%]

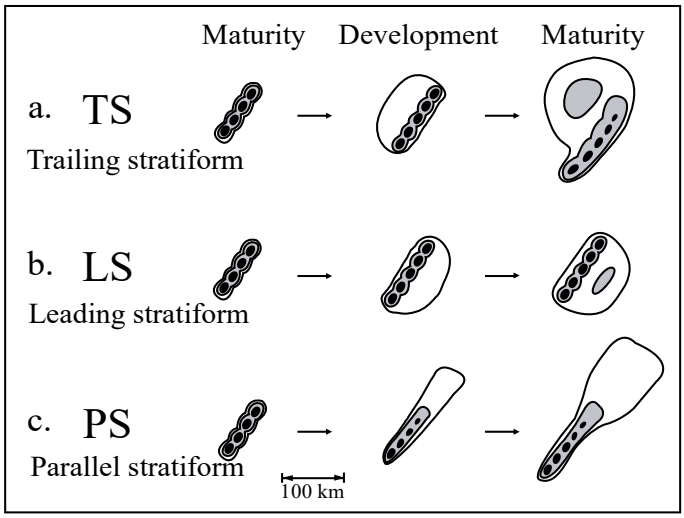

Fig. 9.3: Three types of mesoscale convective lines and their life cycles are classified: (a) convective line with trailing stratiform precipitation (TS); (b) convective line with leading stratiform precipitation (LS); and (c) convective line with parallel stratiform precipitation (PS). Approximate time interval between 3 life cycles are 3-4 h for TS, 2-3 h for LS and PS. Levels of shading roughly correspond to 20, 40, and 50 dBZ. (After Parker and Johnson 2000) [Lin 2007]

Figure 9.4 is a conceptual model in the mature stage of a mesoscale convective line:

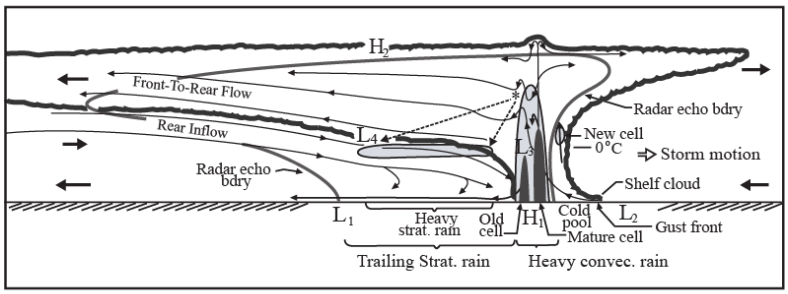

Major features of the TS mesoscale convective lines are:

(1) The trailing straitiform rain is not present during the formation and intentification stages.

(2) The leading cloud overhang and precipitation depends on the the strength of the environmental wind shear.

(3) The front-to-rear flow is located above the rear inflow and advects rearward ice particles falling from the convective cells.

(4) The ice particles collect smaller ice particles and aggregate each other to form large snow aggregates that melt at 0°C level to produce bright band radar echoes and a region of heavier stratiform rain directly below.

- The LS system mentioned above could be further classified into *front-fed LS* (FFLS) and *rear-fed LS* (RFLS), which are sustained by inflow of high-θ_e air from ahead and behind the system, respectively.

Three most common flow structures for observed mesoscale convective lines are: front-fed TS, front-fed LS and rear-fed LS (Parker and Johnson 2004a). They are dynamically unique, and the front-fed TS and the rearfed LS convective lines have some similar characteristics. Even though there are some differences between the front-fed LS and rear-fed LS, they are kinematically similar and the flow circulations are more or less mirror images of each other. The basic structure of LS convective lines is similar to that of the deep-shear model (Fig. 9.1a) except that it contains a front-to-rear flow or jet. The flow circulation of the TS type is similar to that of the shallow-shear model (Fig. 9.1b). In fact, the flow circulation associated with LS convective lines represents very well the squall line observed in central Oklahoma on 22 May 1976 as shown in Fig. 6.12. PS convective line circulation looks like a mixture of the LS and TS types, although with much weaker anvil advection in the cross-line direction due to weaker wind in that direction when compared to that in the along-line direction. Based on idealized numerical simulations of FFLS convective lines, it is found that (Parker and Johnson 2004a,b):

(a) The middle- and upper-tropospheric wind shear are important to the updraft tilt and overall structure of the simulated systems;

(b) In time, simulated FFLS convective lines tend to evolve toward a convective line with TS precipitation structure because they tend to decrease the line-perpendicular vertical shear nearby; and
(c) This, along with gradual increases in the system's cold pool strength, contributes to more rearward-sloping updrafts.

In summary, observations and numerical simulations indicate that the flow circulations and precipitation characteristics of a squall line is controlled by the cold pool strength and the environmental shear.
Aside from the flow structure and characteristics of precipitation discussed above, other major surface features of midlatitude squall lines have been observed.

These include:
(a) presquall mesolow ahead of the convective line (L_2 in Fig. 9.4),
(b) squall mesohigh under the convective line (H_1 in Fig. 9.4),
(c) wake low associated with the trailing stratiform rain area (L_1 in Fig. 9.4), and
(d) mesoscale convective (bookend) vortices at the ends of a squall line.

- MCSs may produce *derechos*, which are characterized as severe, straight-line windstorms.

The derecho has been defined to include any family of downburst clusters associated with an extratropical mesoscale convective system, and has been classified into:
(a) *serial derecho*: produced by several separate convective elements and is favored under strong large-scale forcing, and
(b) *progressive derecho*: produced by a single, curved squall line or mesoscale convective system oriented perpendicular to, and with a bulge in the general direction of the mean midtropospheric flow.

Both significant upper-tropospheric shear above 5 km and low-level shear play important roles in maintaining the strength of long-lived squall lines.

Derecho-type systems may produce severe damage swaths of 100 km or more in width and 500 – 1000 km in length.

- A bulging convective line, called a *bow echo* in radar imaging, has the ability to produce strong, diverging outflow and is typically associated with swaths of damaging surface winds near the apex of the bow.

9.1.2 Formation mechanisms

Mesoscale convective systems are initiated in a variety of large-scale environments.

Some form in moist environments with strong wind shear in the form of squall lines or warm-sector rainbands, while others, such as MCCs and a few warm-front rainbands, occur in moist environments with no strong wind shear.

Several common ingredients are found for the formation of squall lines:

(1) an environment with sufficient moisture for the existence of one or more instabilities (e.g., CI and PI)

(2) a mechanical and/or thermal forcing which provides lifting

(3) an environmental vertical shear that will help organize the convective cells or thunderstorms.

In addition to the required upward motion for moist convection, other important effects of large-scale convergence are its ability to bring a wide region of the atmosphere to saturation before convection begins and to continuously destabilize the environment after convection has been initiated.

For example, Fig. 9.5a shows a numerical model simulation of moist convection initiated by momentum forcing associated with large-scale convergence. As noted in subsection 8.4.3, the upward motion is associated with the large-scale convergence near the rigid flat surface through the mass continuity. In the presence of large-scale convergence, the convective system is not as critically dependent on the formation of a low-level cold pool as those initiated by a warm bubble (Fig. 9.5b). The embedded convective cells in Fig. 9.5a appear to be the result of layer lifting, while the single convective cell in Fig. 9.5b appears to be the result of parcel lifting. The potential instability may play a more dominant role in the layer-lifting situation, while the conditional instability may play a more dominant role in the parcel-lifting situation.

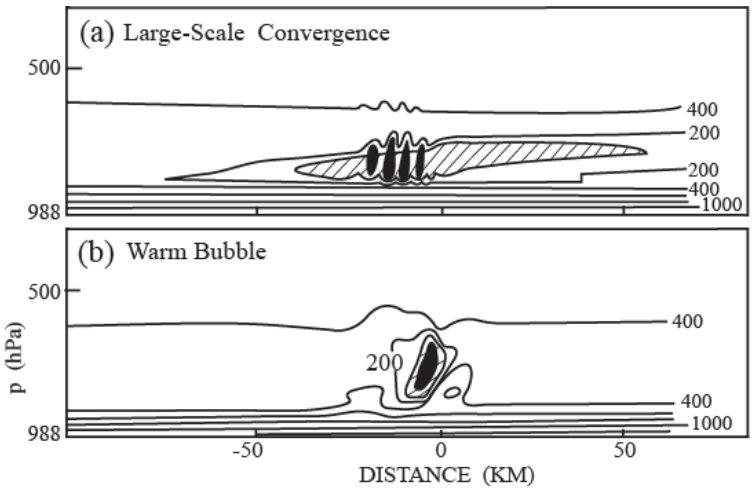

Fig. 9.5: Vertical displacement (m) needed for air to be lifted to its lifting condensation level for moist convection initiated by (a) large-scale convergence and (b) warm bubble. Cloud areas are shaded and regions where the air has to be lifted less than 100 m are hatched. (Adapted after Crook and Moncrieff 1988)

Squall lines may form by:

(1) frontal forcing,
(2) orographic forcing,
(3) thermal forcing,
(4) upper-level forcing,
(5) gravity waves, and
(6) mesoscale instabilities.

Frontal forcing may be associated with either synoptic fronts or mesoscale fronts. Synoptic front forcing is probably the most recognized mechanism of squall line formation. Although both cold and warm fronts can theoretically trigger squall lines, more squall lines are triggered by cold fronts.

Squall lines are often triggered by the ascent of warm, moist, high θ_e air (the so-called *warm conveyor belt*) forced by an

advancing surface cold front in the warm sector of a midlatitude cyclone.

9.1.3 Maintenance mechanisms

Four major mechanisms have been proposed to explain the maintenance of long-lived squall lines:
(a) *three-dimensional effects*,
(b) *gravity wave mechanisms*,
(c) *local balance mechanisms*, and
(d) *forced potential vorticity mechanism*.

a. Three-dimensional effects

When a squall line is composed of supercell storms in a deep, strongly sheared environment, it may be sustained for a significantly longer time. As depicted in the conceptual model (Fig. 9.2), the shear vector forms a large angle to the orientation of the convective line, which prevents the circulations of two adjacent supercells from interfering with each other. In particular, when the shear vector is normal to the line of forcing, it is favorable for the maintenance of a squall line with isolated supercells at either end (Bluestein and Weisman 2000). Thus, the longevity of a squall line in a deeply sheared environment is dependent on the non-interference of three-dimensional supercell storms embedded in the squall line, as in Fig. 9.2. A squall line of this type, which contains three-dimensional, persistent supercells and an anvil that spread downshear in strong upper-level westerlies, has been observed in previous studies (Fankhauser et al. 1992). In this particular case, the environmental wind shear was linear at about 4 ms^{-1} km^{-1} through the troposphere. Although this three-dimensional maintenance mechanism of squall lines theoretically provides a reasonable interpretation of squall line longevity, most squall lines are not composed of supercell thunderstorms (Bluestein and Jain 1985). In this case, the squall lines may be maintained by other mechanisms as described below.

b. Gravity wave mechanism

Convective heating can produce a series of forced internal gravity waves. These waves can, in turn, generate regions of low-level convergence and divergence. The resulting concentration of convection into convergent regions provides a coherent driving mechanism for the wave itself. In this manner, the convection provides the energy and the wave provides the scale selection and organization of convection, thus creating a self-sustaining convective system, also known as a wave-CISK system. This interaction may explain the longevity of mesoscale convective systems. As depicted in Fig. 4.20, the wave packet consists of one convergent and one divergent region with a dominant wavelength comparable to the scale of the squall line or mesoscale convective system. Convective plumes develop in the convergent region, passing into the divergent region as they decay and produce precipitation. When the squall line or the mesoscale

convective system moves at the same speed as the region of surface convergence or the forced gravity waves, then the latent heating can be supported by the upward vertical motion produced by the surface convergence in a coherent manner. The weakness of this mechanism is that many MCSs do not move at the speed of the internal gravity waves.

c. Local balance mechanism

As discussed in Section 8.3, the RKW theory may be used to explain the longevity of a squall line. Based on the RKW theory, the vorticity produced by the density current may counter that produced by the low-level shear on the downshear side of a convective line. Ideally, the long-lived (optimal) state is characterized not by a long-lived cell, but by a long-lived system of convective cells that are constantly generated at the gust front on the downshear side.

In order to elucidate the effects of shear and cold pool interaction on the structure of squall line, three-dimensional simulations in variable surface-based unidirectional shear flow are shown in Figs. 9.7 and 9.8. The basic flow is assumed to have zero velocity at the surface, which increases linearly from 0 to 10, 20, and 30 ms^{-1}, but remains uniform above 5 km. A line thermal in a homogeneous state initiates the convection. In the case of no vertical shear, i.e. $\Delta U = 0\ ms^{-1}/5km$ (Figs. 9.7a and 9.8a), the convective cells are scattered, highly disorganized, and short-lived behind the gust front. When the shear increases to $\Delta U = 10\ ms^{-1}/5\ km$, the simulated squall line is more organized and tilted in the lower layer upshear (leftward in the figure; Fig. 9.7b). In the upper layer, a branch is extended from the upshear-tilted updraft over the density current, while another branch of the updraft is tilted downshear.

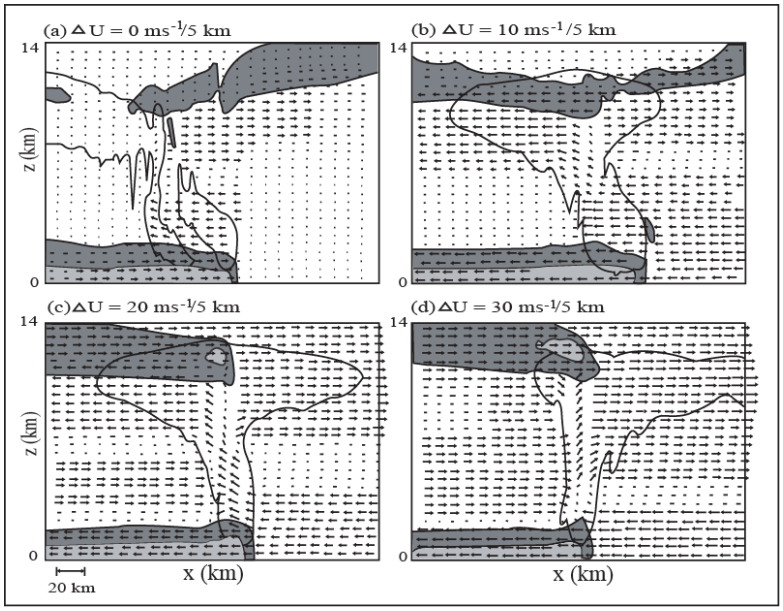

Fig. 9.7: Effects of shear and cold pool interaction on the structure of a convective line after 4-h as illustrated through simulations for a series of three-dimensional idealized numerical experiments with variable strength of surface-based shear flow. The convection is initialized by a line heat source in a homogeneous state characterized by a single profile of temperature and moisture, as used by Weisman et al. (1988). Line-averaged system-relative flow vector wind field, negative buoyancy field (shaded), and outline of the cloud field (thick line) on a vertical cross section through the convective line are shown for different shear strengths: (a) $\Delta U = 0$ ms^{-1}, (b) $\Delta U = 10$ ms^{-1}, (c) $\Delta U = 20$ ms^{-1}, and (d) $\Delta U = 30$ ms^{-1} in the lowest 5 km. Buoyancy values between -0.01 and -0.1 ms^{-2} are darkly shaded and values less than -0.1 ms^{-2} are lightly shaded. The horizontal domain plotted is 240 km. (After Weisman and Rotunno 2004)

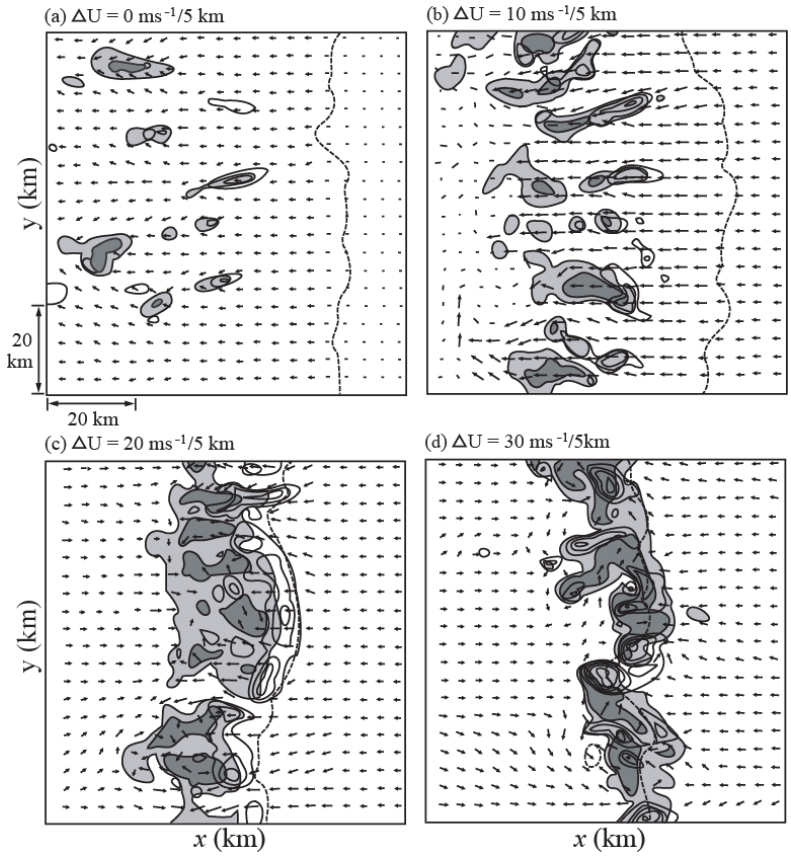

Fig. 9.8: Same as Fig. 9.7 except that this figure shows the system-relative flow vector wind, rainwater mixing ratio, and positive vertical velocity fields on the horizontal cross section at z = 3 km. The vertical velocity is contoured at an interval of 3 ms^{-1} (solid lines) and the rainwater is lightly shaded for 0.001 to 0.004 g kg^{-1} and darkly shaded for rainwater greater than 0.004 g kg^{-1}. The gust front or cold pool boundary is depicted by $\theta' = -1$ K (dashed line). The domain plotted is 80 km x 80 km. (After Weisman and Rotunno 2004)

9.1.4 Squall line movement

Squall line movement is mainly controlled by the following three mechanisms:

(1) advection,
(2) externally forced movement, and
(3) internally forced movement.

Observed external forcing include convergence associated with cold fronts, rainbands, sea-breeze fronts, and gravity waves.

The third mechanism is also referred to as *autopropagation* (Cotton and Anthes 1989).

9.1.5 Rainbands

- A cloud and precipitation system that produces an elongated rainfall pattern is called a *rainband*.
- Rainbands are often convective in nature and often difficult to distinguish from squall lines.

- Six types of rainbands have been identified to form within extratropical cyclones (Houze 1981):
  (1) *warm-frontal rainbands,* located either ahead of or straddling the warm front and have a width of about 50 km;
  (2) *warm-sector rainbands,* typically up to 50 km wide, located in the warm sector and oriented parallel to the surface cold front;

(3) *wide cold-frontal rainbands,* oriented parallel to the cold front and either straddle or are behind the surface cold front, and have a width of about 50 km;
(4) *narrow cold-frontal rainbands*, coincide with the position of the surface cold front and are about 5 km wide;
(5) *prefrontal cold-surge rainbands*, associated with surges of cold air preceding the cold fronts; and
(6) *postfrontal rainbands*, lines of convective clouds that form well behind and generally parallel to the cold front.

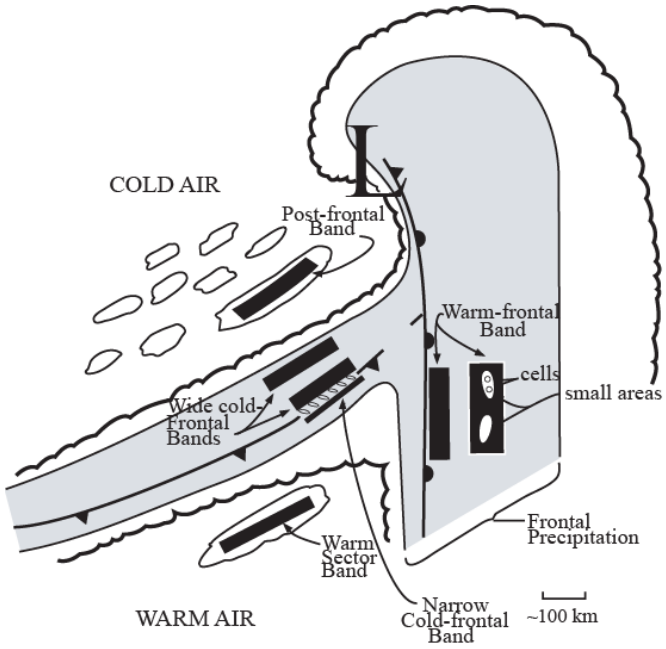

Fig. 9.9: Rainband types associated with a mature extratropical cyclone: (1) warm-frontal rainband; (2) warm-sector rainband; (3) wide cold-frontal rainband; (4) narrow cold-frontal rainband; (5) prefrontal cold-surge rainband; and (6) postfrontal rainband. (Adapted after Houze 1981) [Lin 2007]

Rainbands may also form along other weather systems or near forcing regions. Along with the rainbands discussed above, we may classify the rainbands as the following: (a) *frontal rainbands* (surface and cold front aloft – CFA, see Ch. 10), (b) *cyclone rainbands* (see Sec. 9.3), (c) orographically forced rainbands, and (d) thermally forced rainbands.

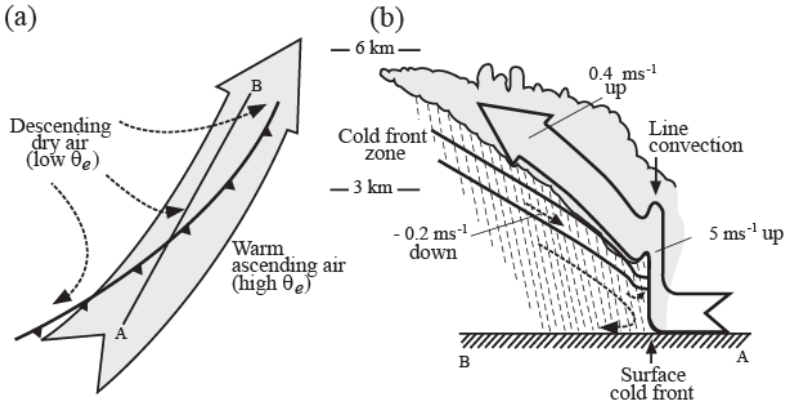

Fig. 9.10: Schematic of airflow and *narrow cold-frontal rainband* in a cold front. (a) horizontal projection. (b) vertical cross section along AB as denoted in (a). Outlined trajectoryies denote flow of warm moist airstream into and through the cloudy zone. Dashed trajectories denote cold, dry airstream. Dashed lines indicate precipitation. Dashed trajectories denote cold, dry airstream. (Adapted after Browning 1986) [Lin 2007]

9.2 Mesoscale convective complexes

9.2.1 General characteristics

- A *mesoscale convective complex* (MCC) is defined as a mesoscale convective system (MCS) that, in satellite observations, exhibits a large, circular, long-lived, and cold cloud shield (Maddox 1980).

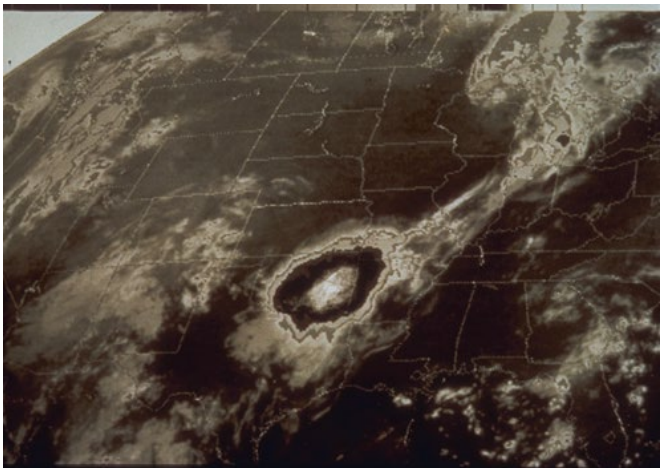

- Based on the infrared satellite imagery and Maddox's definition, the cold cloud shield of an MCC must exhibit the physical characteristics specified in Table 9.1.

Table 9.1: Characteristics of the cold cloud shield of an MCC (Maddox 1980)

Size	A - Cloud shield with continuously low infrared (IR) temperature $\leq$ -32°C must have an area $\geq$ 100,000 km^2. B - Interior cold cloud region with temperature $\leq$ -52°C must have an area $\geq$ 50,000 km^2.
Initiate	Size definitions A and B are first satisfied.
Duration	Size definitions A and B must be met for a period $\geq$ 6 h.
Maximum extent	Contiguous cold cloud shield (IR temperature $\leq$ -32°C) reaches maximum size.
Shape	Eccentricity (minor axis/major axis) $\geq$ 0.7 at time of maximum extent.
Terminate	Size definitions A and B no longer satisfied.

The criteria are selected to identify very large and long-lived MCCs.

Figure 9.11 shows a typical satellite view of an MCC with key infrared enhancement levels and corresponding temperature ranges.

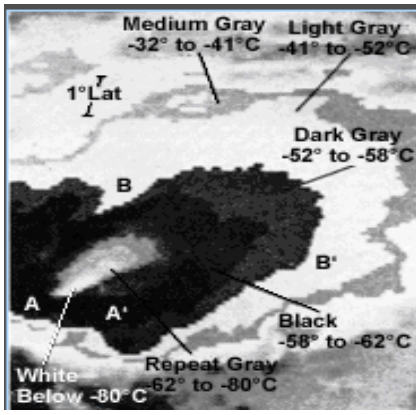

Fig. 9.11: Example of satellite view of an MCC with key infrared enhancement levels and corresponding temperature ranges. See Table 9.1 for the definition of MCC. (After Maddox 1980) [Lin 2007]

- For MCCs over the Central United States, the cloud shield reaches a typical size of 200 000 km^2 for a temperature threshold of -52ºC and the averaged lifetime is about 15 h. Occasionally an MCC can last for several days.

- MCCs may produce widespread rainfall that accounts for a significant portion of the growing-season rainfall over much of the United States corn and wheat belts (Fritsch et al. 1994), local intense rainfalls, widespread damaging winds, flash flooding, severe convective phenomena, such as tornadoes, hail, wind, and intense thunderstorms.

Based on the composite analysis of the synoptic settings of MCCs over the Great Plains of the U.S., the synoptic environment conducive to the MCC genesis may be summarized as:

1) A broad trough exists over the western states, a ridge over the southeast, and a weak high over the Great Lakes;
2) A weak surface front, with a pronounced, southerly low-level jet transports warm, moist (high θ_e) air into the region (Fig. 9.12a);
3) Strong warm air advection is present at all of the lower levels of the atmosphere;
4) Conditionally unstable air over a large region is located ahead and to the right of the advancing MCC. Layer lifting of a potentially unstable air over synoptic front may also provide the low-level forcing;
5) At 700mb, winds typically veer and weaken with height (Fig. 9.12b);
6) Normally a downwind trough signal with weak upwind shortwave moving into the initiation area;
7) The 500 mb flow characteristically out of the southwest, with an increase in wind gradient from south to north (Fig. 9.12c);
8) A weak jet streak to the north of the genesis region on 200 mb flow (Fig. 9.12d); and
9) Characteristically weak diffluent 200 mb-flow over the genesis region.

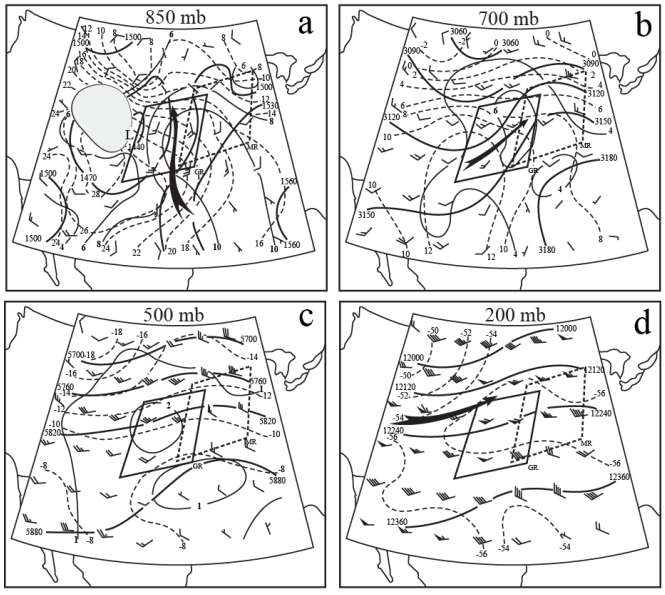

Fig. 9.12: Synoptic environment conducive to MCC genesis, based on the composite analysis of the synoptic settings of MCCs over the Great Plains of the U.S. Height (m, heavy solid contours), isotherms (°C, dashed), and winds (full barb = 5 ms^{-1}, flag = 25 ms^{-1}) on (a) 850 mb. Dark arrow shows axis of maximum winds; (b) 700 mb; (c) 500 mb; and (d) 200 mb. The shaded region in (a) indicates terrain elevations above the 850 mb level. (Adapted after Maddox 1983) [Lin 2007]

Fig. 9.13: Tracks of MCCs documented during 1978-82 for the period of May 16-31. MCC initiated at locations at the beginning of the solid lines and terminated at the end of the solid lines denoted by x. The MCC "initiation" and "termination" are defined in Table 9.1. The "maximum extent" of the MCCs is circle-numbered. Dotted line denotes tracks of a developing thunderstorm prior to MCC initiation. (After Maddox et al. 1986) [Lin 2007]

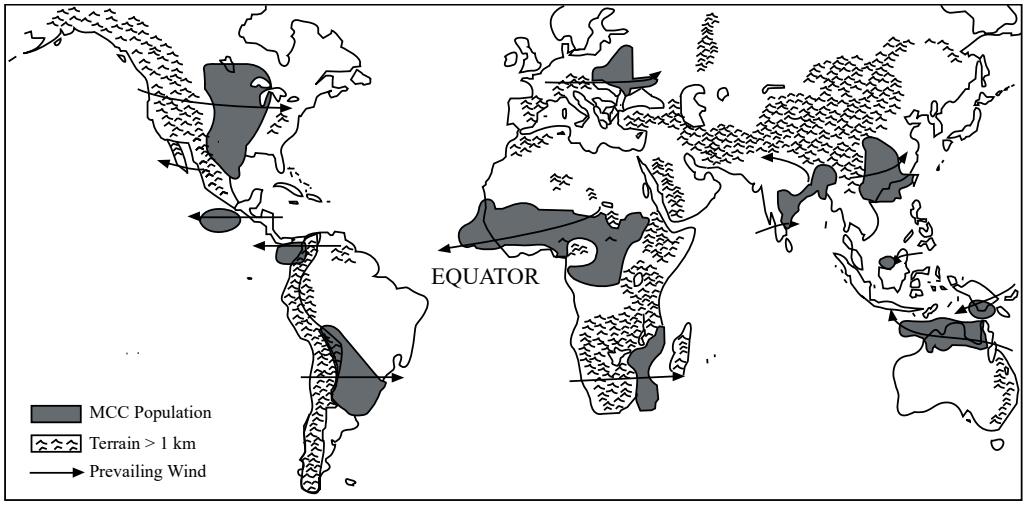

Fig. 9.14: Relationship among MCC population centers, elevated terrain, and prevailing mid-level flow. (After Laing and Fritsch 1997) [Lin 2007]

During the *mature stage*, as mentioned above, an MCC is characterized by a warm-core updradt with an embedded mesoscale convective vortex, a cold-core anticyclone near the tropopause, and a cold, divergent mesohigh due to outflow near the surface. The warm advection pattern shifts eastward across the Great Plains as low-level winds increase and veer (turn clockwise) during the night, while low to mid-level convergence is associated with a strong upward mass flux. Note that the veering and increase of the mean wind is associated with warm advection through the thermal wind relstionship, $\boldsymbol{V}_T = (R/f)\ln(p_1/p_2)(k \times \nabla \overline{T})$, where $\boldsymbol{V}_T$ is the thermal wind velocity, p_1 and p_2 are the lower- and upper-level pressures of the layer, and $\overline{T}$ is the mean temperature of the layer. The mesoscale environment reflects the intense convection. A deep, warm-core updraft develops, which is, in turn, overlain by an intense anticyclonic outflow. The *decay stage* of the MCC results from moving into a more stable and convectively less favorable environment. During its lifecycle, the MCC produces a chilled surface mesohigh, a deep, moist tropospheric layer, an amplified midlevel short-wave, and a cold anticyclonic outflow. The modified environment may persist for several days and affect the evolution of meteorological features over much of the Eastern United States, and this lifecycle definition is similar to that for some Oklahoma squall lines (Ogura and Chen 1977).

MCCs have been documented not only in the Central Plains of the United States, but also in other parts of the world (Laing and Fritsch 1997), such as Central and South America, the western Pacific region and Australia, the Indian subcontinent, Europe, and Africa. Understanding the formation and propagation of MCCs may help meteorologists forecast heavy rainfall, often a precursor to flash flooding, especially over the western Pacific region, and Europe. A significant number of tropical cyclones that have occurred over the eastern Atlantic Ocean, particularly near the Cape Verde Islands, can be traced back to the African continent as MCCs. Thus, understanding the formation and development of MCCs over northern Africa around 10^{o} N has important implications in elucidating the dynamics of tropical cyclogenesis over the tropical eastern Atlantic Ocean.

9.2.2 Formation and development mechanisms

- Observations show that many MCCs in the United States originate from thunderstorm activity over the Rocky Mountains or their eastern slopes.

A three-stage conceptual model of orogenic MCC formation may be proposed (Fig. 9.15):

(1) Stage I: A dry mountain-plains solenoidal (MPS) circulation develops over the lee slope. A group of deep convective clouds forms over the mountain peak (Fig. 9.15a).

(2) Stage II: These deep convective clouds organize into a meso-β-scale convective system, which moves eastward. The meso-β-scale convective system expands into a meso-α-scale convective system while it is moving eastward (Fig. 9.15b).

(3) Stage III: The meso-α-scale convective system continues to grow. As the scale of the unsteady MCS increases to be larger than the Rossby radius of deformation, it becomes more geostrophically balanced and a meso-α-scale upward motion is induced because of geostrophic adjustment (Fig. 9.15c).

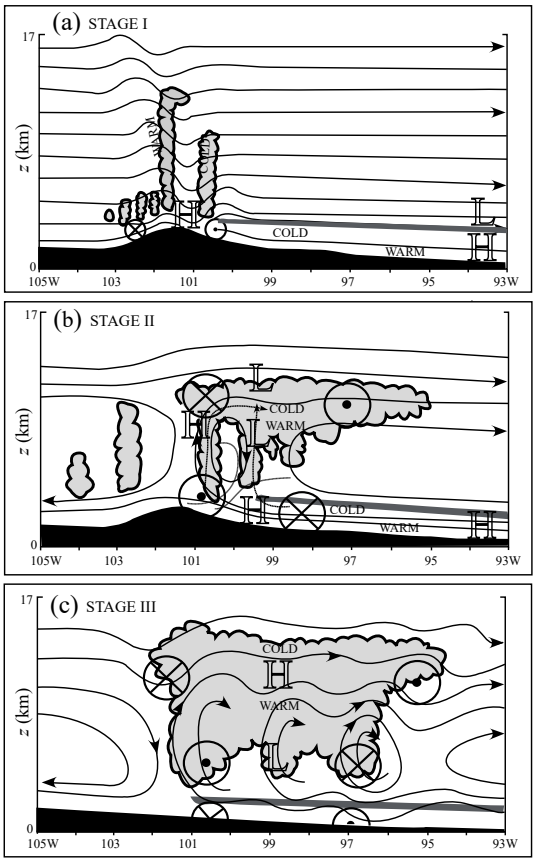

Fig. 9.15: A three-stage conceptual model of orogenic MCC formation: (a) Stage I, (b) Stage II, and (c) Stage III. See text for details. Topography is dark-shaded and the plain inversion is grey-shaded. Regions of clouds are light-shaded. Circles denote flow perpendicular to the plane (X: into the page, • : out of the page). The high and low pressure perturbations are denoted by H and L, respectively, while the cold and warm perturbations are also denoted. (Adapted after Tripoli and Cotton 1989) [Lin 2007]

- MCCs forming over the Rockies tend to do so early in the afternoon, moving eastward into the central Great Plains by the middle of the night and being advected by the mean wind of the mid-tropospheric (e.g., 700-500 hPa) layer. The low-level nocturnal southerly jet provides moisture and unstable airstream as well as lifting through warm air advection, which may help explain the prevalent occurrence of MCCs at night. Figure 9.13 shows the

tracks of MCCs documented during 1978-82 from May 16 to May 31. Some of the MCCs form over the Rocky Mountains, while the remaining form over the Great Plains. Only a few MCCs in the United States form over the Gulf of Mexico. A similar situation occurs in other parts of the world. For example, approximately 30% of the MCCs in South America formed over the eastern slopes of the Andes, whereas the rest developed over the plains of the Plata River basin.

- The tendency for MCCs to be concentrated only in preferred regions, such as in the United States, South America, Africa, India, China, and Australia, suggests that the large-scale environment in these regions must be structured in a fashion that favors the formation of these convective weather systems. In fact, the MCC genesis environments for regions outside North America are very similar and exhibit many of the same dynamic and thermodynamic structures (Laing and Fritch 2000). In the western Pacific region, areas favorable to MCC genesis are: (i) northern Australia, (ii) New Guinea, (iii) northeast India/Bangladesh, (iv) mainland China, and (v) South China Sea (Miller and Fritsch 1991). In summary, MCC systems in most regions tend to form: (1) in the lee of mountain ranges (Fig. 9.14), (2) over land in areas frequented by low-level jets which transport high-θ_e air, and (3) where convective available potential energy is large relative to surrounding areas. MCCs in the tropical easterlies tend to form in the Sahelian region west of the North African mountains, while MCC genesis in the midlatitude westerlies occur east of the South African escarpment (Laing and Fritsch 1993). These mountain ridges are still able to initiate convection, although they are lower than mountains in the Americas and Tibet. Many African MCCs tend to develop over mountains, merge with lee vortices, and embed within African easterly waves and could even be traced to the Ethiopian Highlands (e.g., Fig. 9.22).

  Based on the dynamical mechanism responsible for producing the convection and the large cold cloud shields, an MCC may be categorized into two types. Type 1 results when a mesoscale ribbon of low-level potentially unstable air is forced to ascend in a frontal or baroclinic zone. Type 2 occurs in more barotropic environments and depends on the moist-downdraft production of a surface-based cold pool. The interaction between the cold pool and the ambient vertical wind shear produces mesoscale ascent, as discussed in Section 8.3, and the associated large stratiform cloud shield characteristic of MCCs. In either case, the genesis region must have CAPE to release the conditional instability, layer lifting to release the potential instability, mechanical and/or thermal forcing which helps trigger individual thunderstorms, and a synoptic or mesoscale disturbance that helps organize the thunderstorms into a larger convective system.

Dynamically, an MCC has a Rossby number on the order of 1 and exhibits a horizontal scale comparable to the *Rossby radius of deformation*. Similar to (4.2.12), the Rossby radius of deformation for a circular motion in a stratified fluid may be defined as (Schubert et al. 1980):

$$L_R = \frac{NL_z}{(\zeta + f)^{1/2}(2V/R + f)^{1/2}}, \qquad (9.2.1)$$

where ζ is the vertical relative vorticity, and V the tangential wind speed at the *radius of local curvature* R of the circulation. Observational analysis indicates a dynamic radius of about 300 km. The L_R estimated from numerical simulations suggests that MCC is an inertially stable

balanced MCS (Olsson and Cotton 1997). The unbalanced flow is found to be composed largely of divergent circulations of gravity waves. MCSs typically develop a strong positive vorticity maximum and associated potential vorticity anomaly in the lower and middle troposphere. As an MCC develops this positive vorticity maximum, it achieves greater inertial stability, and hence a smaller L_R. The inertial stability is associated with the horizontal restoring force that resists lateral displacement and typically takes about three to six hours for the Coriolis effects to become significant at midlatitudes. Based on the above discussion of MCC genesis, stage III is characterized by a significant transformation from an unsteady MCS with a scale smaller than L_R into a more balanced MCC with a scale larger than the Rossby radius of deformation, although the convection is still characterized by multicells, i.e. the convection is still unsteady. The CAPE released in the deep convection in an MCS excites gravity waves. However, for an MCS with a scale larger than L_R, most of the gravity wave energy is confined locally within the storms and is projected into the rotational flow.

Figure 9.16 depicts the structure and development mechanism of the mesoscale convective vortex (MCV) in a mature MCC, which includes a shallow, cold, long-lived anticyclone in the lower troposphere (below 850 hPa), a strong updraft with a warm core, an MCV with low pressure in the middle troposphere, and a large, cold, shallow, short-lived anticyclone with high pressure in the upper troposphere. The conceptual model for mature MCCs was constructed, based on the forced potential vorticity theory of Raymond and Jiang (1990), on the assumption of an environment with a low-level jet and a deep layer of weak flow and weak shear in the middle and upper troposphere (Fritsch et al. 1994). Below the level of maximum low-level jet (e.g., 850 mb), the strengthening of shear-induced vorticity and cold pool-induced vorticity on the upshear (left) side of the cold pool will produce an overtaking flow tilted more downshear (rightward) over the cold outflow surface. Thus, the overtaking air over the cold ouflow would be unlikely to reach its level of free convection (LFC) in the rear (upshear) of the cold pool until it flows isentropically into the interior of the convective system. Once the air parcel reaches its LFC inside the convective cloud, it would flow more vertically due to the buoyancy. Thus, the overtaking air can initiate new convection beneath the PV maximum and the convective system can feed from the rear (left hand side in Fig. 9.16) instead of the front.

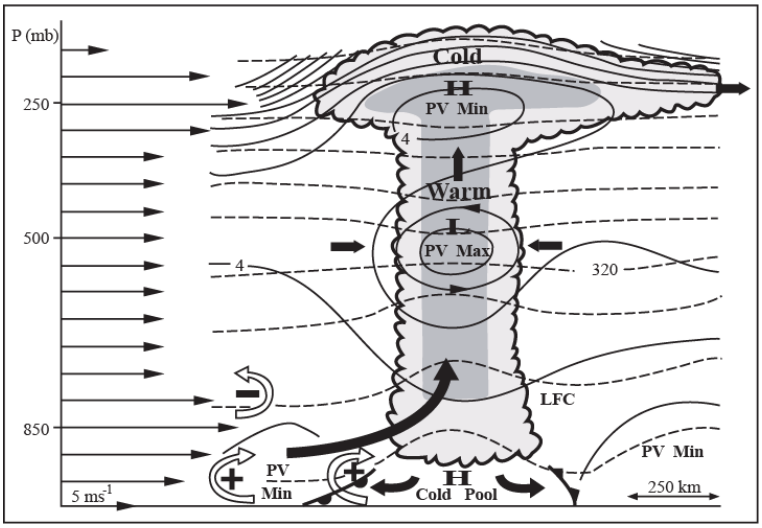

Fig. 9.16: A conceptual model of the structure and development of the mesoscale warm core vortex of a mature MCC. Thin arrows along the ordinate denote the environmental wind. Open arrows with either a plus or a minus sign denote the sense of the horizontal vorticity generated by the environmental wind shear and cold pool. Thick solid arrows indicate the wind inside and around the convective system. Frontal symbols depict outflow boundaries. Dashed lines are potential temperature (5 K intervals) and solid lines are potential vorticity (PV) (interval of 2 x 10^{-7} $m^2s^{-1}K$ kg^{-1}). The convective system is propagating from left to right at about 5 to 8 ms^{-1} and is being overtaken by high-θ_e air in the low-level jet. Air overtaking the vortex ascends through isentropic surfaces, reaches its level of free convection (LFC), thereby initiating deep convection (shaded). (Adapted after Fritsch et al. 1994, Thiao et al. 1993, and Jiang and Raymond 1990) [Lin 2007]

The structure of PV and temperature anomalies depicted in Fig. 9.16 can be interpreted by considering the Ertel's PV definition

$$q = \frac{1}{\rho}\left[(\boldsymbol{\omega} + f\boldsymbol{k})\cdot\nabla\theta\right], \tag{9.2.2}$$

and the PV tendency equation,

$$\frac{Dq}{Dt} = \frac{1}{\rho}\left[\left(\boldsymbol{\omega} + f\boldsymbol{k}\right)\cdot\nabla\dot{\theta} + \nabla\mathrm{x}\boldsymbol{F}\cdot\nabla\theta\right], \tag{9.2.3}$$

where $\boldsymbol{F}$ is the frictional force vector and $\dot{\theta}$ is the diabatic heating rate. Neglecting the frictional force, the PV tendency describing cumulus convection may be approximated by

$$\frac{Dq}{Dt} \approx \left(\frac{\zeta + f}{\rho}\right)\frac{\partial\dot{\theta}}{\partial z}. \tag{9.2.4}$$

Assuming the diabatic heating associated with cumulus convection has a maximum at the midtroposphere, a pair of positive and negative PV anomalies will result below and above the maximum heating level, respectively. This, in turn, will generate a pair of cyclonic and anticyclonic circulations in the lower and upper parts of the MCC, respectively.

MCVs have been observed in the mature-to-decaying MCCs as well as in tropical mesoscale convective systems. A MCV embedded within a tropical MCC has a warm core similar to that of a tropical cyclone and may provide an enhanced inertial stability that makes the diabatic heating more efficient in producing a balanced, rotational flow (Olsson and Cotton 1997). The cyclonic circulation associated with the mesoscale vortex embedded within the MCC at the midtroposhere is related to the development of a stratiform precipitation region that accompanies the MCC (Johnson and Bartels 1992). A midtropospheric short-wave propagating in the ambient flow is able to further enhance the diabatic processes by organizing the thunderstorms and increasing the background relative vorticity. Note that the above *MCV generation mechanism* differs from that responsible for the vortices (which are also called *bookend vortices*) depicted in Fig. 9.8c, in which the MCVs are formed by the titling of either ambient or baroclinically(cold-pool)-generated horizontal vorticity at the ends of finite-length convective lines. Once an MCC moves into a region with unfavorable conditions for sustaining its convection, the desintegration of the MCC is inevitable. As the system dissipates, the precipitation intensity and rate continue to decrease, but the strong upward motion and cyclonic circulation in the midtroposphere and anticyclonic circulation in the upper troposphere may still persist during the early part of the MCC dissipation stage.

An accurate quantitative precipitation forecast accompanying an MCC is heavily dependent on a successful forecast of the MCC's movement. In this regard, the movement of the radar-observed meso- β scale convective elements (MBEs) embedded within the MCC, rather than the movement of the cold cloud shield centroid, is more responsible for the heaviest rainfall. The movement of an MCS is composed of the sum of an advection component and a propagation component. The advective component is controlled by the mean motion of the convective cells or the mean flow in the deep tropospheric layer (roughly between 850 to 300 mb). The propagation component depends on the rate and direction at which the new convective cells are growing, which is, in turn, related to the low-level jet shear and the cold pool.

[For reference only]

9.3 Tropical cyclones

9.3.1 General characteristics

Tropical cyclones (TCs) are non-frontal synoptic-scale "warm-core" low-pressure systems that originate over the tropical or subtropical oceans and contain organized deep convection and a well-defined cyclonic surface wind circulation. Since the radius of gale-force winds of a mature tropical cyclone is about several hundred km and the radius of intense convection and strong winds is about 100 km, tropical cyclones may also be viewed as mesoscale convective systems. Although the cloud and precipitation characteristics are similar to those of mesoscale convective systems, as discussed in previous sections, moist convection associated with a tropical cyclone is strongly linked to the *tropical cyclone vortex*, which arises from convergence of planetary vorticity. The centrifugal force plays a significant role in the force balance in such a system since it has very high wind speeds and relatively small horizontal scales. To a first approximation, the radial pressure gradient force, Coriolis force, and centrifugal force in a quasi-steady-state tropical cyclone vortex are in *gradient wind* balance. In addition to strong horizontal winds, excessive rain produced by deep convection, supported by the presence of a deep layer of very moist air (e.g., $q_v > 20$ g kg^{-1}, where q_v is the water vapor mixing ratio) and strong upward motion with vertical velocity exceeding 1 ms^{-1} produced by strong convergence, may cause flooding and landslides. The average rainfall rate in the radial ring of about 200 km is about 100 mm d^{-1}, but the maximum rainfall rate may exceed 500 mm d^{-1}. Despite the damage that the high winds and extremely heavy rainfall tropical cyclones may bring, the rainfall supplied by weak and moderate hurricanes or typhoons are essential to agriculture and fresh water supply to some areas.

Tropical cyclones tend to affect the eastern and equatorward portions of the continents. Figure 9.17 shows genesis locations and tracks of tropical cyclones with wind speeds of at least 17 ms^{-1} for the period of 1995-2004. Based on intensity, tropical cyclones in the Atlantic, eastern and western Pacific are classified as a *tropical depression* for a weaker system with $V_{max} \le 17$ ms^{-1} (~ 62 km h^{-1} ~ 38 mph), a *tropical storm* for a moderate system with 18 ms^{-1} $\le V_{max} \le$ 32 ms^{-1}, and a *hurricane* or *typhoon* for a strong system with $V_{max} \ge 33$ ms^{-1}. Hurricanes are called *major hurricanes* when $V_{max} \ge 50$ ms^{-1} (~178 km h^{-1} ~ 111 mph) and typhoons are classified as *supertyphoons* when $V_{max} \ge 67$ ms^{-1} (~241 km h^{-1} ~ 150 mph). The maximum wind speed of a strong tropical cyclone may exceed 100 ms^{-1}, which may produce storm surge by driving an ocean rise of several meters along the coast.

The characteristics of tropical cyclones differ from those of *extratropical cyclones* in many ways. Tropical cyclones derive their energy from sensible and latent heat fluxes from the ocean; while the extratropical cyclones derive their energy from available potential energy associated with baroclinicity. Because tropical cyclones are barotropic, they are more symmetric and circular than extratropical cyclones which are often associated with cold fronts, warm fronts and occluded fronts. During the development stage, tropical cyclones are oriented vertically, while extratropical cyclones are normally tilted into the prevailing shear. Structurally, tropical cyclones have their strongest winds near the earth's surface, while extra-tropical cyclones have their strongest winds near the tropopause. This is caused by the thermal wind balance responding to the warm core of tropical cyclones and the cold core of extra-tropical cyclones. A tropical cyclone may transform into an extratropical cyclone as it interacts with midlatitude baroclinicity (e.g., Atallah and Bosart 2003). Occasionally, an extratropical cyclone may lose its frontal

features, develop convection near the center of the storm and transform into a full-fledged tropical cyclone (e.g., Davis and Bosart 2003). Such a process is most common in the North Atlantic and Northwest Pacific basins.

9.3.2 Tropical cyclogenesis

Tropical cyclogenesis is often preceded by some disturbances or precursors, such as *easterly* (*tropical*) *waves*, *African easterly waves* (*West African disturbance lines* – WADLs), *tropical upper tropospheric troughs* (TUTTs), and old frontal boundaries. Once a disturbance forms and sustained convection develops, it can become more organized and eventually evolve into a tropical depression given an abundant supply of heat and moisture from the ocean, background cyclonic vorticity associated with the Earth's rotation, preexisting disturbance with sufficient vorticity, and weak wind shear. Several necessary conditions for tropical cyclogenesis have been proposed (e.g., Riehl 1948; Palmén 1948; Gray 1968, 1998):

(1) A warm and large body of ocean water of at least 26.5ºC, throughout a sufficient depth at least 50 m to provide the thermal energy for the tropical cyclone;
(2) Sufficiently large planetary vorticity, i.e. a distance of at least 500 km from the equator, so that the near gradient wind balance can occur;
(3) A near-surface preexisting disturbance with sufficient vorticity and convergence, such as easterly waves, to generate a convergent low-level wind, triggering convection, and helping to organize and sustain the mesoscale convective systems and cloud clusters;
(4) Divergence associated with an upper-level trough overlaying the low-level cyclonic disturbance to enhance and sustain the deep upward motion;
(5) A potentially unstable atmosphere to allow the heat stored in the ocean to be released for the tropical cyclone development;
(6) Relatively moist middle troposphere for allowing the continuous development of widespread thunderstorm activity; and
(7) Weak vertical wind shear, with less than 10 ms^{-1} between the ocean surface and the tropopause, to avoid the disruption of the vertical development of deep convection around the cyclone center.

The formation of tropical cyclones differs significantly from that of extratropical cyclones. A tropical cyclone forms through complicated scale interactions between the small-scale cumulus clouds, mesoscale organization of cumulus clouds, and large-scale environment. Tropical cyclone formation is one of the most challenging problems in dynamic meteorology and has been studied since 1940s. Since the early 1960s, several major mechanisms have been proposed to explain tropical cyclogenesis: (a) cooperative intensification mechanism, (b) linear CISK mechanism, (c) wind-induced surface-heat exchange (WISHE) mechanism, (d) vortex interaction mechanism, and (e) hot-tower mechanism. These mechanisms will be discussed as follows.

a. Cooperative intensification mechanism

A cooperative intensification mechanism between cumulus convection and moisture convergence in the planetary boundary layer of a quasi-balanced cyclonic vortex has been proposed to explain the tropical cyclogenesis (Ooyama 1964, 1969). This cooperative intensification mechanism assumes the release of latent heat by moist convection given off by the conditionally unstable moist air at the bottom of the vertical column. The cooperative intensification mechanism includes the following processes:

(1) The heating effects of deep cumulus clouds are represented in terms of a mass flux from the boundary layer to upper layer wherever there is resolved-scale boundary-layer convergence.
(2) The deep cumuli will entrain ambient air from the middle layer as they rise through it and detrain in the upper layer.
(3) The entrainment rate is determined as a function of time to satisfy energy conservation, assuming that the air detrained into the upper layer follows the saturation equivalent potential temperature of ambient air in that layer.
(4) Although a relatively large amount of CAPE is used in the initial sounding in a nonlinear model incorporating this mechanism (Ooyama 1969), this is not required for the mechanism to work (Dengler and Reeder 1997).

This mechanism is illustrated in Fig. 9.18a. The nonlinear model simulations, based on cooperative intensification mechanism, demonstrated that (a) the latent and sensible heat fluxes from the warm ocean were crucial to vortex intensification and that (b) the progressive reduction of the local Rossby radius of deformation occurs as the inertial stability of the TC vortex increases in the inner-core region. The latter effect is nonlinear, and helps reduce the scale separation between the deep cumuli and the balanced tangential circulation of the vortex, so that the individual cumuli become more and more under the control of the balanced dynamics.

b. Linear CISK mechanism

A linear *Conditional Instability of the Second Kind* (*CISK*) mechanism has been proposed to explain tropical cyclogenesis (Charney and Eliassen 1964), which includes the following processes: (1) The latent heat released by cumulus convection produces a lower-tropospheric cyclonic disturbance in the environment. (2) The disturbance, in turn, produces low-level moisture convergence through boundary layer friction (i.e., Ekman pumping). (3) The low-level convergence then lifts the conditionally unstable boundary layer air to the level of free convection and leads to the release of latent heat. In this linear CISK mechanisn, the latent heating is represented by the vertical velocity at the level of free convection (z_b),

$$\dot{Q} = \frac{-gL}{c_p T_o}\frac{Dq_{vs}}{Dt} \approx \frac{-gL_v}{c_p T_o}\frac{\partial q_{vs}}{\partial z} w' , \tag{9.3.1}$$

where L_v is the latent heat of condensation and q_{vs} is the saturated mixing ratio of water vapor. The above equation is then substituted into the thermodynamic equation to yield

$$\frac{\partial b'}{\partial t} + N_m^2 w' = 0 , \tag{9.3.2}$$

where b' is the perturbation buoyancy ($g\theta'/\theta_o$), $w'(z_b) = w_b'$, and

$$N_m^2 = \frac{g}{\bar{\theta}_e^*}\frac{d\bar{\theta}_e^*}{dz} \approx \frac{g}{\theta_o}\frac{d\bar{\theta}_e}{dz} + \frac{gL_v}{c_p T_o}\frac{\partial q_{vs}}{\partial z} . \tag{9.3.3}$$

In the above equation, N_m is the *moist buoyancy frequency* defined as $N_m^2 = (g/\bar{\theta}_e^*)(d\bar{\theta}_e^*/dz)$, where $\bar{\theta}_e^*$ is the saturation equivalent potential temperature of the environmental air. This represents a self-exciting process as illustrated in Fig. 9.18b.

The Charney-Eliassen linear CISK theory received wide support for explaining tropical cyclogenesis for more than two decades after it was proposed in the early 1960s, but has suffered heavy criticism since the early 1980s (e.g., Ooyama 1982; Emanuel 1994; see review in Smith 1997). The major deficiencies of the Charney-Eliassen linear CISK mechanism are as follows.

(1) The heating function (9.3.1) is not supported by the fact that the θ_e of rising air does not increase with increasing vertical motion. (2) The growth rates of CISK unstable modes are rather uniform over a broad range of horizontal scales. (3) The theory fails to take into account the nonlinear processes that are needed to explain the dynamics of a mature tropical cyclone. (4) The representation of cumulus heating is unable to capture the feedback of convection on the large-scale flow.

c. WISHE mechanism

In light of the drawbacks of linear CISK theory, it has been proposed that tropical cyclone intensification results from a finite-amplitude instability involving the feedback between the cyclone and WISHE (Emanuel 1986). In other words, a tropical cyclone can intensify and maintain its circulation against dissipation entirely by self-induced anomalous fluxes of *moist enthalpy* from the sea surface with virtually no contribution from preexisting CAPE. The *specific enthalpy* is defined as $h = c_p T + L_v q_v$ and the change in *enthalpy* becomes $\delta h = c_p \delta T + L_v \delta q_v$.

The energy cycle of a mature tropical cyclone is analogous to a *Carnot heat engine*, as illustrated in Fig. 9.19. The energy cycle of a mature tropical cyclone consists of the following four processes: isothermal expansion (with the addition of enthalpy), adiabatic expansion, isothermal compression, and adiabatic compression. Imagine that an air parcel moves from the outer region near sea surface toward the eyewall along Leg 1 (a to b in the figure), it experiences a drop in pressure and an increase in sensible and latent heat fluxes. This will induce an increase in *moist entropy*. The change in moist entropy (δs) can be calculated from the following relationship:

$$T\delta s = c_p \delta T - \alpha \delta p + L_v \delta q_v . \qquad (9.3.4)$$

Equation (9.3.4) indiates that lowering surface pressure while maintaining air temperature near the sea surface ($\delta T = 0$) will lead to an increase of moist entropy, assuming that $\delta q_v = 0$. In the mean time, frictional force exerted by the sea surface decreases the angular momentumas the air parcel spirals in along Leg 1. Leg 1 is regarded as an isothermal expansion process as in the Carnot cycle because the temperatures are nearly constant ($\delta T = 0$). At the eyewall (b in Fig. 9.19), the flow turns upward and closely follows surfaces of constant entropy and angular momentum as it ascends upward and outward near the storm top along Leg 2 (b to o). Leg 2 can be approximately regarded as an adiabatic expansion process in a Carnot cycle. In reality, an air parcel would exchange entropy and momentum with its environment due to mixing. Thus, the tropical cyclone is actually not a closed cycle. Along leg 3 (o to o'), the air parcels lose entropy by radiation acquired along Leg 1 and gain angular momentum by mixing with the environment when individual parcels are descending and mixing with the environmental air. Leg 3 is entirely isothermal, and can be regarded as an isothermal compression process as in Carnot cycle. The *Carnot cycle* is closed by leg 4 (o' to a in Fig. 9.19). Along leg 4, the angular momentum is conserved, although entropy is lost and gained. The irreversible entropy source is produced in its entirety by mixing of moist and dry air. Leg 4 can approximately be viewed as an adiabatic compression process.

The WISHE mechanism is consistent with the cooperative intensification mechanism discussed above. Numerical simulations (Rotunno and Emanuel 1987) demonstrated that a hurricane-like vortex indeed amplifies as a result of air-sea interaction instability in an atmosphere that is neutral to cumulus convection (i.e. no CAPE). Figure 9.20 shows a

numerically simulated idealized tropical cyclone at the mature stage, which depicted the detailed core structure reasonably well. The subsidence in the eye with its maximum around the inner edge of the eyewall originates from the returning flow at the top of the eyewall (Figs. 9.20a-c). The motion in the radial-vertical plane of the mean cyclone is mainly along the constant absolute angular momentum surface (Fig. 9.20d), consistent with the WISHE mechanism. The cyclone has a warm core with a maximum temperature anomaly of about 18ºC at about 300 hPa (Fig. 9.20e). The maximum PV (Fig. 9.20f) is located just inside the radius of maximum wind (RMW), below about 800 hPa, which is due to concentration of PV associated with convective heating in the eyewall, and these features appear to be realistic.

The difference between the cooperative intensification mechanism and WISHE mechanism appears to be the degree of emphasis placed by the respective authors on the relative importance of convection and surface fluxes in the intensification of hurricanes (Smith 1997). The physics implied in the cooperative intensification and WISHE mechanism should be represented in contemporary models if the heat transfer between convection and air-sea interaction heat is to be properly treated.

d. Vortex interaction mechanism

The vortex interaction mechanism, as originally proposed by Fujiwhara (1921), was revived in the early 1990s and has been evolving since then. Since a two-dimensional turbulent flow has a tendency to form finite-amplitude, coherent vortex structures in the absence of external forcing, a random distribution of vorticity will concentrate into isolated vortices due to an upscale merger process in which smaller vorticity perturbations in the flow merge into a larger one. This provides a potential mechanism for the development and growth of mesoscale vortices and initial development of tropical cyclones in the atmosphere in the absence of thermal forcing. Thus, tropical cyclogenesis can arise from a constructive interaction between the larger-scale environmental and mesoscale vortex dynamics (Ritchie and Holland 1993; Hendricks et al. 2004). Figure 9.21 shows an example of this type of vortex interaction mechanism, in which two low-level vortices (LLC1 and LLC2) merged to form a tropical depression, which eventually developed into Typhoon Irving (1992). Note that this mechanism may produce a precursor vortex, but convection is still required for amplification.

e. Hot-tower mechanism

A pre-existing surface vortex of finite amplitude or sufficient strength is needed for tropical cyclogenesis to occur via the WISHE mechanism. Observations indicate that cumulus convection is an essential ingredient for tropical cyclogenesis because tropical cyclones form out of mesoscale convective complexes that are embedded in tropical or easterly waves. Thus, the WISHE theory implicitly assumes that a transformation of a tropical disturbance to a surface vortex of sufficient strength has already taken place (Montgomery and Farrell 1993). The problem arises from how a weak-amplitdue tropical disturbance is transformed into a finite-amplitude surface vortex, assuming that WISHE mechanism works. Since this is still a current topic of research, a brief summary is only appropriate.

Based on numerical simulations, it has been proposed that *vortical* tall cumulonimbi with strong vertical vorticity, are important ingredients for forming tropical cyclones via the following two-stage evolutionary processes. (1) Multiple small-scale cyclonic PV towers are generated by latent heat release in the lower troposphere and (2) multiple mergers of convectively generated PV or vorticity anomalies from the hot towers (Hendricks et al. 2004). In the first stage, a pulsing

and locally enhancing cyclonic PV is produced by the latent heat release within the hot tower in the lower troposphere, as indicated by (9.2.4). Note that the PV generation is dominated by the vertical gradient of diabatic heating. In other words, the strong updrafts in the hot towers converge and stretch existing low-level vorticity into intense small-scale vortex tubes. A 64 PVU (1 PV unit = 1 x 10^{-6} $m^2 s^{-1} K\ kg^{-1}$) may be produced in the layer of z = 0 to 5 km, $\partial\dot{\theta}/\partial z = 45\,\mathrm{K\ h^{-1} km^{-1}}$, $\zeta = 10^{-3}\,\mathrm{s^{-1}}$ and $\rho = 0.7\,\mathrm{kg\ m^{-3}}$. In the second stage, multiple mergers of these cyclonic anomalies occur. The merger is enhanced by the *vortex axisymmetrization* process which means that the decay of the asymmetries favor the creation of a master vortex.

Hot towers might develop in a TC precursor, such as the MCS shown in Fig. 9.22. The MCS developed in the lee of the Ethiopian Highlands (EH) (see subsection 9.2.2). This MCSs was embedded in an African eastery wave and traveled across the African continent. The convective vortices or hot towers associated with the MCS might have served as a precursor for the tropical depression over the eastern Atlantic Ocean that eventually became Hurricane Alberto (2000).

f. Preexisting disturbances and a unified mechanism for tropical cyclogenesis

There is a growing body of evidence suggesting that tropical cyclogenesis in the eastern Pacific Ocean occurs in association with *easterly waves* that have been produced over the African continent and propagated across the Atlantic and Caribbean and into the eastern Pacific (Molinari and Vollaro 2000). We must note that this area is on the lee side of the mountains in Mexico and Central America. The westward moving waves may include different types of synoptic-scale waves, such as mixed Rossby gravity waves, equatorial Rossby waves, and off-equatorial Rossby waves. In some tropical cyclogenesis cases in the eastern Pacific Ocean, tropical cyclones started with orographically generated lee cyclones. In addition to the westward propagating waves, it has been observed that tropical cyclogenesis over the eastern Pacific on the lee side of the Mexican and Central American mountains are often associated with other eastward moving or stationary systems, such as the Madden-Julian (1994) oscillation (MJO), ITCZ, monsoon trough, or any long-period, slowly moving diabatic heating disturbance.

The MJO is characterized by an eastward propagation of large areas of both enhanced and suppressed tropical rainfall, observed mainly over the Indian Ocean and Pacific Ocean. The oscillation period is approximately 30-60 days. For example, a large-amplitude mixed Rossby-gravity wave packet during 1987 lasted 5 weeks and spawned three tropical cyclones in the western Pacific Ocean, one with each cyclonic gyre within the wave packet as the gyres turned away from the equator in the western Pacific (Dickinson and Molinari 2002; Aiyyer and Molinari 2003). The dynamics of the interactions of the mixed Rossby-gravity waves and the MJO, and their interactions with sea surface temperature anomaly (SSTA) and topography are complicated (e.g., Hsu and Lee 2005), and deserve further investigation. The significance of these larger-scale waves and their interactions with topography lies in the fact that they provide cyclonic vorticity in a broader region for cyclogenesis to occur. This indicates that the tropical cyclogenesis over the western Pacific basin may be predicted a week or earlier in advance, if the geneses of these synoptic waves and background flow can be identified. Thus, emphasis should be placed in the investigation of the interaction of easterly waves, eastward propagating disturbances, SSTA and orography.

Based on the above description, it appears that some of the above mechanisms may work cooperatively and sequentially to form a tropical cyclone. A unified mechanism for tropical cyclogenesis may work as follows:

(1) A TC precursor begins as an MCS that forms and is embedded within easterly waves over the land or ocean;
(2) These easterly waves with MCS embedded propagate over the ocean may interact with other systems, such as MJO, monsoon trough, ITCZ or Kelvin wave. The TC genesis region must also possess other key ingredients, including high SST, weak vertical wind shear, and away from the equator;
(3) The cumuli embedded in the MCS develop further into vortical hot towers via the hot-tower mechanism;
(4) These hot towers, or convective vortices associated with the MCC, may also interact with other vortices and merge to form a larger, isolated, cyclonic vortex via the vortex interaction mechanism;
(5) Once the surface wind speeds exceed a certain threshold, and if the disturbance is of sufficient size, then the vortex will develop further into a tropical cyclone via the WISHE/cooperative intensification mechanism if other conditions are met.

g. Control parameters of tropical cyclogenesis

The necessary conditions and formation mechanisms discussed above suggest the following control parameters (Gray 1998):

(1) f (Coriolis parameter)
(2) ζ (low-level relative vertical vorticity)
(3) S (tropospheric vertical wind shear)
(4) E (ocean thermal energy, manifested as ocean temperatures greater than 26°C to a depth of 60 m)
(5) $\Delta\theta_e$ (difference in θ_e between the surface and 500 mb), and
(6) RH (relative humidity in the middle troposphere),

which can be combined into a *dynamic potential* ($f\zeta / S$) and a *thermal potential* [$E(\Delta\theta_e)RH$]. Multiplying both dynamic and thermal potentials gives a *seasonal TC genesis parameter*. Calculations of this parameter from climatological data appear to be well correlated with the regions of long-term frequency of occurrence of global tropical cyclogenesis (McBride 1995). A *genesis parameter* for evaluating the potential for eastern Atlantic tropical cyclogenesis, which includes the effects of vertical wind shear, *barotropic-baroclinic instabilities*, and mid-level moisture variable controlling entrainment of environmental air, has also been proposed (DeMaria et al. 2005). This genesis parameter appears to be useful for the prediction of tropical cyclogenesis over the eastern Atlantic Ocean. Some common ingredients discussed above were not included in this genesis parameter and could be very useful if a universal set of necessary conditions or nondimensional control parameters for tropical cyclogenesis were to be proposed.

h. Extratropical hurricanes

Storms that are similar to tropical cyclones in structure sometimes occur over extratropical oceans. These storms possess special characteristics usually found in tropical cyclones, such as their occurrence within deep moist adiabatic atmospheres, the small, intense vortices with clear eyes surrounded by deep cumulonimbi, and the presence of warm cores with strong surface winds. These extratropical cyclones, which form over relatively warm water during the winter and possess tropical cyclone characteristics, are known as "*extratropical hurricanes"* (Bergeron 1954). In particular, some polar lows and Mediterranean cyclones are named, respectively,

"*arctic hurricanes"* (Emanuel and Rotunno 1989) and "*Mediterranean hurricanes"* (Emanuel 2005).

Polar lows are small synoptic-scale or subsynoptic-scale cyclones forming during the cold season within polar or arctic air masses over open sea, such as the Bering Sea and the Baltic Sea. Typically, they are several hundred kilometers in diameter, and often possess strong winds. Unlike tropical cyclones, some polar lows tend to form in highly baroclinic environments, such as to the north of major frontal zones, and are preceded by strong upper-tropospheric troughs or lows. Typically, satellite imagery of polar lows shows spiral or comma cloud patterns, and sometimes reveals an inner eye and warm core similar to that of tropical cyclones. Although some polar lows have maximum surface winds of 30 ms^{-1}, they normally do not possess hurricane or typhoon strength winds ($V_{\max} \geq 33\, ms^{-1}$).

Numerical studies indicate that both the baroclinic processes and surface fluxes play roles in the polar low formation. Since the environments conducive to polar low formation vary to a certain extent, different mechanisms have been proposed to explain their formation, which include (1) CISK mechanism (e.g., Rasmussen 1979), (2) baroclinic instability (e.g., Reed 1979), (3) WISHE (Emanuel and Rotunno 1989), and (4) coupled forcing mechanism (Montgomery and Farrell 1992; to be explained below). The first and third mechanisms are related to those proposed for tropical cyclogenesis, as discussed earlier in this subsection. The CISK mechanism does not fully describe the polar low formation as well as it does for tropical cyclogenesis.

Baroclinic instability is a well-known mechanism used to explain extratropical cyclogenesis. However, many e-folding timescales, i.e. several days, are usually required in order to have the most unstable normal mode of baroclinic instability develop to intensities of observed polar lows. Observations indicate that the time for rapidly developing polar lows to attain their mature stage can be as short as one day. The WISHE mechanism for tropical cyclogenesis may also explain polar lows, thus proposing that they are indeed arctic hurricanes (Emanuel and Rotunno 1989). The smaller radii of polar lows are due to larger values of the Coriolis parameter, i.e. smaller λ_R. Similar to tropical cyclones, surface flux-driven polar lows require sufficiently well developed disturbances to initiate the air-sea interaction intensification process. The coupled forcing mechanism for polar low development consists of two stages (Montgomery and Farrell 1992). In the first stage (induced self-development), a mobile upper-level trough initiates a rapid low-level circulation in a conditionally neutral baroclinic atmosphere. In the second stage (diabatic destabilization), the development is associated with the production of low-level potential vorticity through latent heat release. The WISHE mechanism helps explain the relatively short (about 1 day) spinup timescale for polar lows, and it appears that polar lows may require more than one mechanism to spin up and that the dominant mechanism(s) is(are) analogous to those involved in tropical cyclogenesis.

9.3.3 Intensity and mesoscale structure

Once a tropical cyclone reaches its *mature stage*, it is maintained by the extraction of sensible and latent heat fluxes from the warm ocean and the transport of the heat released by cloud formation upward to the upper troposphere, as discussed in the previous subsection. At this stage, it consists of mesoscale features such as the *eye*, *eyewall(s)*, *spiral rainbands*, secondary vortices, and upper-level outflow and cloud shields (Fig. 9.23a). The surface winds spiral inward cyclonically and upward toward the center, forming an *outer vortex* with spiral cloud and rainbands. The most intense rain and winds occur in the eyewall, which surrounds a nearly symmetric circular eye with downward motion, clear sky, and light winds. Occasionally,

multiple *concentric eyewalls* occur, in which the outer eyewall may contract and replace the *inner eyewall*. Most, but not all, tropical cyclones with maximum winds in excess of 40 ms^{-1} have eyes visible on satellite imagery. Eye diameters vary from 10 to more than 100 km and average about 30 km. A nearly circular and symmetric spiral current composes the overall wind field associated with a tropical cyclone, in a moving frame of reference.

a. Intensity of a mature tropical cyclone

Prediction of tropical cyclone intensity is extremely important due to the associated high wind and torrential rain. In spite of advanced observational techniques and numerical weather prediction models developed in the past several decades, improvement of intensity prediction is still limited, especially compared with the numerical prediction of tropical cyclone tracks, and remains challenging.

The winds within a mature tropical cyclone can be assumed to be in *gradient wind balance*. This force balance can be expressed in the cylindrical coordinates as

$$\frac{V^2}{r} + fV - \frac{1}{\rho}\frac{\partial p}{\partial r} = 0, \tag{9.3.5}$$

where V is the tangential wind speed and r is the radial distance from the rotating axis of the cyclone. The first, second, and third terms of (9.3.5) represent the centrifugal force, Coriolis force, and pressure gradient force in the radial direction, respectively. Applying the equation of state to (9.3.5) leads to

$$\frac{V^2}{r} + fV = RT\frac{\partial \ln p}{\partial r}. \tag{9.3.6}$$

Thus, if the tangential velocity is known at a certain location away from the cyclone center, the pressure reduction can be roughly estimated if the averaged temperature in the area encircled by a radius r is used. On the other hand, if the radial pressure gradient is known at certain location, then the tangential velocity can be estimated by assuming a constant averaged temperature.

The surface pressure reduction associated with a tropical cyclone cannot be attributed solely to the latent heat released by cumulus convection (Riehl 1948). It is well recognized that the major additional energy source is the sensible and latent heat (with condensation) fluxes from the ocean surface. These heat fluxes may be represented by the moist entropy change, (9.3.4), which indicates that lowering surface pressure while maintaining air temperature near the sea surface will lead to an increase of moist entropy (assuming that $\delta q_v = 0$) for an air parcel that moves from the outer region near sea surface toward the eyewall along Leg 1 of Fig. 9.19. The moist entropy is also related to the equivalent potential temperature (θ_e) by

$$T\,\delta s \approx c_p T\,\delta \ln \theta_e. \tag{9.3.7}$$

Thus, increasing moist entropy leads also to an increase of θ_e. The high θ_e air ascends, warms the column, and lower the surface pressure. Based on this concept, the *maximum potential intensity* (MPI) of a tropical cyclone can be estimated by δp by combining (9.3.4) and (9.3.7) (Holland 1997),

$$\delta p = \rho\,[c_p \delta T + L_v \delta q_v - c_p T \delta \ln \theta_e]. \tag{9.3.8}$$

Another approach for estimating the MPI is based on the Carnot cycle concept (Fig. 9.19). The maximum wind speed is approximated by (Emanuel 1997):

$$|V_{\max}|^2 \approx \frac{C_h}{C_D}\left(\frac{T_s - T_o}{T_o}\right)(h_o^* - h), \tag{9.3.9}$$

where C_h and C_D are the exchange coefficients for enthalpy and momentum, respectively, T_s the sea surface temperature, T_o the mean temperature of Leg 3 of the TC Carnot cycle, h the moist enthalpy, and h_o^* the saturated (with respect to T_s) moist enthalpy of air near the sea surface. The middle term on the right hand side of (9.3.9) has a form similar to the thermodynamic efficiency, $\varepsilon = (T_s - T_o)/T_s$, except that it has the output temperature in the denominator, which reflects the added contribution from the *dissipative heating*. The dissipative heating can be approximated by

$$D_h = C_D \rho |V|^3. \tag{9.3.10}$$

The dissipative heating represents the heat gained by the viscous dissipation of turbulence kinetic energy. Equation (9.3.9) provides an estimate of *MPI* in terms of maximum tangential wind velocity. The minimum pressure of a tropical cyclone can be estimated by assuming an air parcel that ascends moist adiabatically from the level of free convection to the undisturbed top of a mean tropical atmosphere. The pressure difference between the storm center and ambient atmosphere of a tropical cyclone can be estimated by

$$\delta p_c \approx -\left(\frac{c_p \overline{p}}{R}\right)\left(\frac{T_b - T_o}{T_b}\right)\frac{\delta\theta_{ec}^*}{\overline{\theta}_e}, \tag{9.3.11}$$

where overbars denote the ambient values, T_b is the temperature at the cloud base or top of the boundary layer, T_o is the outflow temperature, and $\delta\theta_{ec}^*$ is the difference of saturation equivalent potential temperature at the storm center.

Prediction of tropical cyclone intensity remains challenging. For example, in the formulation of (9.3.8), a large ambient CAPE may be produced by raising the surface temperature while keeping the remainder of the sounding the same. This may lead to the estimate of an unrealistic low surface pressure (Camp and Montgomery 2001). In the mean time, the formulation of (9.3.11) may lead to an estimate of MPI that is not large enough (Persing and Montgomery 2003), and thus, further research is required to resolve the MPI issue. In addition, in simulations of Hurricane Diana (1984), it was found that almost any intensity can be produced by various choices of "model physics", depending on the selection of grid spacing, initialization time, and model physical parameterizations (Davis and Bosart 2002). In addition to the above physical and numerical factors, tropical cyclone intensity is also affected by factors in its environment, such as vertical wind shear and sea surface temperature. Tropical-cyclone intensity can be affected by shear via *ventilation*, where low-level heat and moisture are advected rapidly away in the upper levels. In order to improve the prediction of MPI, further research is required to improve our understanding of tropical cyclone dynamics.

b. Mesoscale structure of a tropical cyclone

The structure of a tropical cyclone is relatively well understood due to the availability of advanced observational instruments and techniques. For example, Fig. 9.23a shows the radar echo pattern seen in Hurricane Alicia, which clearly depicts the principal and secondary rainbands, eyewall, and eye. Figure 9.23b shows six mesovortices, with one located in the center and the other five surrounding it, embedded in the eye of Hurricane Isabel at 1315 UTC 12 September 2003, as revealed in satellite imagery. Theoretical studies indicate that these vortices underwent multiple merger events (Kossin and Schubert 2004). Examples of observed tangential

wind, radial wind, composite mesoscale vertical velocity, and equivalent potential temperature fields for Hurricane Allen (1980) can be found in Fig. 9.24. The descending and ascending motions associated with eye and eyewall, respectively, are clearly depicted. The eyewall expands outward with height. The maximum tangential wind is located near the surface, while the maximum vertical velocity is located at about 3.5 km.

The eye and eyewalls are the most prominent features from satellite and radar imagery of tropical cyclones. Within the eye of a tropical cyclone, the atmosphere is characterized by relative warm, light wind, clear or broken clouds, and low surface pressure. The eye is formed by the adiabatic warming associated with the subsidence of air and is surrounded by the *eyewall*. The eyewall is composed of a ring of cumulonimbus convection, which contains the strongest winds and most intense rainfall of a tropical cyclone. When the core of a tropical cyclone becomes saturated or moist neutral, intensification is controlled by the feedback process between the surface *enthalpy flux* and wind speeds, according to

$$F_h = -C_h \rho |V|(h_o^* - h), \tag{9.3.12}$$

where F_h is the enthalpy flux from the ocean into the atmosphere. The above equation indicates that the surface heat flux increases with increasing surface wind speeds. In the meantime, however, dissipation increases as the cube of wind speed, according to (9.3.10), which eventually balances energy production and leads the tropical cyclone to a quasi-steady state. The spinup time for tropical cyclone vortex may be estimated by dividing the depth scale of the cyclone by the vertical velocity scale, i.e. the time for air to move vertically through the cyclone (Emanuel 1989). The depth of the cyclone scale can be represented by the atmospheric scale height (H). The vertical velocity scale can be estimated by $C_D V_{\max}$, where V_{max} is the maximum wind speed given by (9.3.9). This scale is the same as that which governs surface fluxes (Betts 1983). Combining these two scales together leads to the spinup time scale for a tropical cyclone

$$\tau \approx \frac{H}{C_D V_{\max}}. \tag{9.3.13}$$

Without the subsidence in the warm eye, a tropical cyclone cannot reach a central surface pressure as low as the observed by simply lifting low-level air in the clouds surrounding the eye (Riehl 1954). The subsidence may be explained by the fact that the air detrains from the top of the eyewall clouds and sinks inside the eye due to compensating downward motion. The air in the eye descends to the lower troposphere where it is entrained back to the eyewall. This adiabatic warming contributes to the low pressure inside the eye. The amount of warming can be estimated by following a hypothetical air parcel, which mixes with air from the eyewall, descending through the eye. The downward motion inside the eye of a tropical cyclone may be explained by the following vortex dynamics. Subsidence is driven by an adverse, axial gradient of perturbation pressure that is associated principally with the decay and/or radial spread of the tangential wind field with height. Assuming the TC vortex is in gradient wind balance, the perturbation pressure gradient force at the center of the eye is related to the tangential wind by (Smith 1980):

$$-\frac{1}{\rho}\left(\frac{\partial p'}{\partial z}\right)_{r=0} = \frac{1}{\rho}\frac{\partial}{\partial z}\int_0^R \rho\left(\frac{V^2}{r} + fV\right)dr, \tag{9.3.14}$$

where r is the radius from the vortex center and R is a large radius where perturbation pressure (p') vanishes. The above equation implies that in the layer where tangential wind (V) decreases with height, there exists a downward pressure gradient force. This occurs because the right side

of (9.3.14) is negative in average sense, thus producing subsidence inside the eye of the TC vortex. The buoyancy force due to adiabatic warming almost exactly opposes this pressure gradient force. Observations indicate that stronger downward motion in hurricane eyes occur during their intensifying stage, as implied by thes mechanism described above. The eye also derives its warm temperature through inward advection and detrainment mixing from the eyewall (Holland 1997). Observations also indicate that the air supplying the subsidence originates both at the tops of eyewall cumuli (hot towers) as well as from air detrained out of the adjacent updraft at the midlevels. This deduction is based on Doppler radar observations of subsiding air, with vertical velocities of several meters per second, that descends at least 9 km and extends horizontally nearly 25 km into the eye interior of Hurricane Bonnie (1998) (Heymsfield et al. 2001). Numerical models with fine horizontal resolution are able to simulate the core structure of tropical cyclones reasonably well. Figure 9.25 shows an example of numerically simulated vertical structure and flow circulation around the eye and eyewall of Hurricane Andrew (1992). The basic structures and circulations in and surrounding the eye are consistent with observations.

Observations indicate that the sea level pressure at the center of an intense tropical cyclone is 50–100 hPa lower than outside the vortex, but only 10–30 hPa of the total pressure fall occurs inside the eye between the eyewall and the vortex center (Willoughby 1998). The pressure difference between the eye and eyewall is due to the adiabatic warming associated with dry subsidence inside the eyewall. Figure 9.26 shows a sounding taken by an aircraft inside the eye of Hurricane Olivia (1994), which indicates warm and very dry air aloft, separated by an inversion from cloudy air below. The dewpoint depressions at the inversion level inside eyewall of tropical cyclones, typically 850–500 hPa, are 10–30 K, much less than about the 100 K that would occur if the air descended from tropopause level without dilution by the environmental clouds. However, the observed temperature and dewpoint distribution above the inversion can be derived by sinking an undiluted air dry adiabatically 100 hPa from an initial sounding that is somewhat more stable than a moist adiabat. This indicates that the subsidence of the air trapped inside the eyewall and above the inversion is drawn downward toward the inversion level as the air below it flows outward into the eyewall, as depicted in Fig. 9.27.

When low-level air parcels flow inward and spiral upward along the eyewall, their PV increases rapidly. This may form an annular tower of high-PV air against the low-PV air inside the eye, and produces an area of air that is highly unstable barotropically (Schubert et al. 1999). When the unstable region is perturbed, the vorticity of the eyewall region pools into discrete areas, creating polygonal eyewalls (Fig. 9.23b) and is proposed to be produced by vortex Rossby waves (e.g., Kuo et al. 1999). The *vortex Rossby waves* are Rossby waves that propagate azimuthally on the radial gradient of relative potential vorticity in the cyclonic vortex circulation. The radial PV gradient associated with the vortex motion serves as the restoring force for the vortex Rossby waves, analogous to the PV gradient associated with the β effect for the planetary Rossby waves. Occasionally, mesovortices form within the eye, as shown in Fig. 9.23b. This type of vortex Rossby wave- may play an important role in determining TC structure and intensity changes. Numerical simulations indicate that the maximum growth of the instabilities of the initial flow occurrs at wavenumber 13, and 13 mesovortices are “rolled up” from the vorticity in the eyewall (Kossin and Schubert 2004). As the mesovortices migrate into and around the eye while rotating cyclonically, rapid merger occurs and results in the pentagonal patterns.

A typical hurricane or typhoon consists of an azimuthally averaged symmetric flow and banded asymmetric features. The most prominent banded features associated with a hurricane or

typhoon are the *spiral rainbands*, which are often evident in satellite and radar imagery, such as that shown in Fig. 9.23a. There are a couple of ways to classify the rainbands of tropical cyclones. Based on their motion, they can be classified as either *stationary* or *moving rainbands* (Willoughby et al. 1984). Some stationary rainbands may be interrelated, and are often referred to as *stationary band complex*. The stationary band complex is composed of the *principal band*, the *connecting band*, and the *secondary band*. Figure 9.23a shows an example of radar echo patterns of *principal* and *secondary rainbands*, which are distinct from the eye wall, formed within a hurricane. Another type of rainband associated with a tropical cyclone can be purely stratiform. The stratiform rainband is formed when a plume of ice particles from somewhere along the eyewall falls through the 0ºC level after spiraling outward at upper levels. Based on location and dimension, tropical cyclone rainbands can be classified also as inner and outer rainbands. Two major mechanisms have been proposed to explain the generation of tropical cyclone spiral rainbands: inertia-gravity waves and vortex Rossby waves. In the first mechanism, the TC *spiral rainbands* are considered to be a manifestation of inertia-gravity waves (e.g. Willoughby et al. 1984; Chow et al. 2002). In the second mechanism, the inner bands are considered as *breaking vortex Rossby waves*, and the outer bands as the result of the nonlinear breakdown of the intertropical convergence zone through barotropic instability (e.g., Guinn and Schubert 1993). Therefore, different mechanisms may be responsible for generating different types of TC spiral rainbands.

The cyclonic circulation of a tropical cyclone in the lower troposphere weakens with height, eventually turning into an anticyclonic circulation at the top of the storm, in response to the high pressure built up in the upper troposphere. The TC outflow is quite asymmetric and is often composed of one or two anticyclonically curving jets (e.g., Merrill 1988). Observations show different patterns of the TC outflow, depending upon the interaction of the TC outflow with environmental synoptic flow. The TC outflow provides a channel that carries high potential temperature air from the convective core of the tropical cyclone outward to its far environment, which is then cooled by radiation, as an important process in completing one branch of the tropical cyclone Carnot cycle (Fig. 9.19). The evolution of the tropical cyclone outflow plays important roles in affecting both the TC motion, structural change, and intensity (Holland and Merrill 1984).

9.3.4 Tropical cyclone movement

A tropical cyclone, once it forms, may move as far as several thousand kilometers away from its genesis region. After its formation, a tropical cyclone in the Northern Hemisphere normally moves to the northwest and then recurves to the northeast after moving into the midlatitude westerlies. Prediction of tropical cyclone movement remains one of the most important and challenging tasks in tropical cyclone forecasting. A tropical cyclone's movement is influenced by both large-scale dynamics and its internal dynamics, which are mesoscale in nature. The TC motion is mainly influenced by the following factors: (1) interaction of a TC vortex with an environmental flow or nearby TCs, (2) β-effect, (3) vertical shear, (4) convective heating, and (5) topography.

The fundamental characteristics of TC motion influenced by the interaction between the TC vortex and environmental flow can be understood by considering the nondivergent barotropic vorticity equation on a β plane,

$$\frac{\partial \zeta}{\partial t} = -\boldsymbol{V} \cdot \nabla \zeta - \beta v . \qquad (9.3.15)$$

The last term on the right hand side is the planetary vorticity (f) advection by the meridional flow (v). A local vorticity maximum tends to be advected downstream by the environmental flow, thus the vorticity center of the TC vortex is displaced or steered downstream. Examples of environmental flows in affecting TC motion include the prevailing easterlies in the tropics, prevailing westerlies in the midlatitudes, and winds associated with synoptic systems, such as high pressure systems over Pacific and Atlantic, synoptic fronts, synoptic-scale waves, and even the rotational flow associated with an adjacent tropical cyclone (i.e. the *Fujiwhara* (1921) *effect*, to be explained later). Here, the environmental flows also include mid- and upper-tropospheric flow. These influences may also be dependent on the TC's intensity since the TC may also interact with its environmental flow.

The β-effect on TC movement is associated with the differential advection of planetary vorticity by the meridional wind. This mechanism may be interpreted by considering a vortex in a quiescent fluid, which is depicted in Fig. 9.28. On the west side of the vortex center in the northern hemisphere, northerly wind associated with the rotational flow of the vortex advects larger planetary vorticity from higher latitudes. On the other hand, on the east side of the vortex center, a southerly wind component advects smaller planetary vorticity from lower latitudes. Thus, a local positive (negative) relative vorticity tendency ($\partial\zeta/\partial t$) is produced to the west (east) of the vortex center. This tends to induce a pair of secondary circulations with opposite sense to advect the vortex northward (Fig. 9.28). However, the actual linear numerical solution of (9.3.15) for a vortex in a quiescent fluid only gives a westward dispersion with very little displacement of the vortex, similar to the linear Rossby waves, while the nonlinear solution gives a northwestward movement (Chan and Williams 1987). This phenomenon can be explained by the nonlinear interaction between the vortex and the horizontal gradient of the planetary vorticity. An isolated vortex sitting on the earth's surface tends to produce an asymmetric flow with a dipole structure, which is referred to as a *β-gyre*, as shown in Fig. 9.29. Although the dipole structure of the β-gyre resembles that depicted in Fig. 9.28, the gyres are oriented counterclockwise about 45° from the north-south direction and the pattern is asymmetric. This asymmetric flow in the center, i.e. the *ventilation flow*, is toward the northwest, as can be found by calculating $(u_{as}, v_{as}) = (-\partial\psi/\partial y, \partial\psi/\partial x)$, where the subscript "$as$" denotes asymmetric and ψ is the streamfunction.

In the real atmosphere, the factors affecting the TC movement are complicated by the presence of stratification, latent heat release, friction, vertical wind shear and environmental flow. The environmental flow is strongly influenced by nearby weather systems, tropical cyclones and topography. The potential vorticity, as defined earlier in Section 9.2, can be used to help understand the TC movement because it includes both dynamic and thermodynamic processes. In the presence of the vertical wind shear, the upper-level anticyclonic circulation would be shifted downstream of the shear vector relative to the low-level cyclone. Conservation of PV would cause a downward penetration of the upper-level anticyclone and an upward penetration of the low-level cyclone that creates an additional steering flow, as sketched in Fig. 9.30. Both upward penetration and downward penetration result in northward deflection of the vortex. Latent heating released by the cloud and precipitation formation associated with a tropical cyclone will produce a negative (positive) PV anomaly at upper (lower) levels, which in turn can induce a downward (upward) penetration of the anticyclonic (cyclonic) circulation and affect the TC motion (Wu and Kurihara 1996). In addition to the effects discussed above, a tropical cyclone's movement may also be influenced by a nearby tropical cyclone, known as the *Fujiwhara* (1921) *effect*, inducing a cyclonically rotation around each other due to the interaction

of their outer circulations which may even cause an eventual merger. Once a tropical cyclone makes landfall on a continent, the surface friction tends to weaken and change the direction of tropical cyclone motion. If mountains exist on the continent or island, the movement, intensity, and the primary circulation of a tropical cyclone can be strongly influenced.

References

Aiyyer, A. R., and J. Molinari, 2003: Evolution of mixed Rossby–gravity waves in idealized MJO environments. *J. Atmos. Sci.*, **60**, 2837–2855.

Atallah, E. H., and L. F. Bosart, 2003: The extratropical transitionadn precipitation distribution of Hurricane Floyd (1999). *Mon. Wea. Rev.*, **131**, 1063-1081.

Bergeron, T., 1954: The problem of tropical hurricanes. *Quart. J. Roy. Meteor. Soc.*, **80**, 131-164.

Betts, A. K., 1983: Thermodynamics of mixed stratocumulus layers saturation point budgets. *J. Atmos. Sci.*, **40**, 2655-2670.

Bluestein, H. B., and M. H. Jain, 1985: Formation of mesoscale lines of precipitation: Severe squall lines in Oklahoma during the spring. *J. Atmos. Sci.*, **42**, 1711-1732.

Bluestein, H. B., and M. L. Weisman, 2000: The interaction of numerically simulated supercells initiated along lines. *Mon. Wea. Rev.*, **128**, 3128-3149.

Browning, K. A., 1986: Conceptual models of precipitating systems. Wea. Forecasting, **1**, 23-41.

Bryan, G. H., and J. M. Fritsch, 2000: Moist absolute instability: The sixth static stability state. *Bull. Amer. Meteor. Soc.*, **81**, 1207-1230.

Camp, J. P., and M. T. Montgomery, 2001: Hurricane maximum intensity: Past and present. *Mon. Wea. Rev.*, **129**, 1704-1717.

Carbone, R. E., 1982: A severe frontal rainband. Part I: Stormwide hydrodynamic structure. J. Atmos. Sci., **39**, 258-279.

Chan, J. C. L., and R. T. Williams, 1987: Analytical and numerical studies of the beta-effect in tropical cyclone motion. Part I: zero mean flow. *J. Atmos. Sci.*, **44**, 1257-1265.

Charney, J. G., and A. Eliassen, 1964: On the growth of the hurricane depression. *J. Atmos. Sci.*, **21**, 68-75.

Chow, K. C., K. L. Chan and A. K. H. Lau. 2002: Generation of Moving Spiral Bands in Tropical Cyclones. *J. Atmos. Sci.*, **59**, 2930–2950.

Cotton, W. R., and R. A. Anthes, 1989: *Storm and Cloud Dynamics*. Academic Press, 883pp.

Crook, N. A., and M. W. Moncrieff, 1988: The effect of large-scale convergence on the generation and maintenance of deep moist convection. *J. Atmos. Sci.*, **45**, 3606-3624.

Davis, C. A., and L. F. Bosart, 2002: Numerical simulations of the genesis of Hurricane Diana (1984). Part II: Sensitivity of track and intensity prediction. *Mon. Wea. Rev.*, **130**, 1100-1124.

Davis, C. A., and L. F. Bosart, 2003: Baroclinically induced tropical cyclogenesis. *Mon. Wea. Rev.*, **131**, 2730-2747.

Dengler, K., and M. J. Reeder, 1997: The effects of convection and baroclinicity on the motion of tropical-cyclone-like vortices. *Quart. J. Roy. Meteor. Soc.*, **123**, 699-725.

DeMaria, M., M. Mainelli, L. K. Shay, J. A. Knaff and J. Kaplan. 2005: Further improvements to the statistical hurricane intensity prediction scheme (SHIPS). *Wea. Forecasting,* **20**, 531–543.

Dickinson, M., and J. Molinari, 2002: Mixed Rossby-gravity waves and western Pacific tropical cyclogenesis. Part I: Synoptic evolution. *J. Atmos. Sci.*, **59**, 2183-2196.

Elsberry, R. L. (Ed.), 1995: *Global Perspective of Tropical Cyclones*. WMO-/TD No. 693, World Meteor. Org., 289pp.

Emanuel, K.A., 1986: An air-sea interaction theory for tropical cyclones. Part I: Steady state maintenance. *J. Atmos. Sci.*, **43**, 585-604.

Emanuel, K. A., 1989: The finite-amplitude nature of tropical cyclogenesis. *J. Atmos. Sci.*, **46**, 3431-3456.
Emanuel, K. A., 1994: *Atmospheric Convection*. Oxford University Press, New York, 580pp.
Emanuel, K. A., 1997: Some aspects of hurricane inner-core dynamics and energetics. *J. Atmos. Sci.*, **54**, 1014-1026.
Emanuel, K. A., 2005: Genesis and maintenance of "Mediterranean hurricanes". *Adv. Geosci.*, **2**, 217-220.
Emanuel, K. A., and R. Rotunno, 1989: Polar lows as arctic hurricanes. *Tellus*, **41A**, 1-17.
Fankhauser, J. C., G. M. Barnes, and M. A. LeMone, 1992: Structure of a midlatitude squall line formed in strong unidirectional shear. *Mon. Wea. Rev.*, **120**, 237-260.
Fiorino, M., and R. L. Elsberry, 1989: Some aspects of vortex structure related to tropical cyclone motion. *J. Atmos. Sci.*, **46**, 975-990.
Fritsch, J. M., J. D. Murphy, and J. S. Kain, 1994: Warm core vortex amplification over land. *J. Atmos. Sci.*, **51**, 1780-1807.
Fujiwhara, S., 1921: The mutual tendency towards symmetry of motion and its application as a principle in meteorology. *Quart. J. Roy. Meteor. Soc.*, **47**, 287-293.
Grady, R. L., and J. Verlinde, 1997: Triple-Doppler analysis of a discretely propagating, long-lived, High Plains squall line. *J. Atmos. Sci.*, **54**, 2729-2748.
Gray, W. M., 1968: Global view of the origin of tropical disturbances and storms. *Mon. Wea. Rev.*, **96**, 669-700.
Gray, W. M., 1998: The formation of tropical cyclones. *Meteor. Atmos. Phys.*, **67**, 37-69.
Guinn, T., and W. H. Schubert, 1993: Hurricane spiral bands. *J. Atmos. Sci.*, **50**, 3380-3404.
Hendricks, E. A., M. T. Montgomery, and C. A. Davis, 2004: The role of "vortical" hot towers in the formation of tropical cyclone Diana (1984). *J. Atmos. Sci.*, **61**, 1209-1232.
Heymsfield, G. M., J. B. Halverson, J. Simpson, L. Tian, and T. P. Bui, 2001: ER-2 Dopper radar investigations of the eyewall of Hurricane Bonnie during the convection and moisture experiment-3. *J. Appl. Meteor.*, **40**, 1310-1330.
Hill, C. M., and Y.-L. Lin, 2003: Initiation of a mesoscale convective complex over the Ethiopian Highlands preceding the genesis of Hurricane Alberto (2000). *Geophys. Res. Lett.*, **30**, 1232, doi:10.1029/2002GL016655.
Holland, G. J., 1983: Tropical cyclone motion: environmental interaction plus a beta-effect. *J. Atmos. Sci.*, **40**, 328-342.
Holland, G. J., 1997: The maximum potential intensity of tropical cyclones. *J. Atmos. Sci.*, **54**, 2519-2541.
Holland, G. J., and R. T. Merrill, 1984: On the dynamics of tropical cyclone structural changes. *Quart. J. Roy. Meteor. Soc.*, **110**, 723-745.
Houze, R. A., Jr., 1981: Structures of atmospheric precipitation systems – A global survey. *Radio Sci.*, **16**, 671-689.
Houze, R. A., Jr., S. A. Rutledge, M. I. Biggerstaff, and B. F. Smull, 1989: Interpretation of Doppler weather-radar displays in midlatitude mesoscale convective systems. *Bull. Amer. Meteor. Soc.*, **70**, 608-619.Hsu, H.-H., and M.-Y. Lee, 2005: Topographic effects on the eastward propagation and initiation of the Madden-Julian oscillation. J. Climate, 18, 795-809.
Jiang, H., and D. J. Raymond, 1995: Simulation of a mature mesoscale convective system using a nonlinear balance model. *J. Atmos. Sci.*, **52**, 161-175.

Johnson, R. H., and D. L. Bartels, 1992: Circulations associated with a mature-to-decaying midlatitude mesoscale convective system. Part II: Upper-level features. *Mon. Wea. Rev.*, **120**, 1301-1320.

Jorgensen, D. P., 1984: Mesoscale and convective scale characteristics of mature hurricanes. Part I: Inner core structure of Hurricane Allen (1980). *J. Atmos. Sci.*, **41**, 1287-1311.

Kossin, J. P., and W. H. Schubert, 2004: Mesovortices in Hurricane Isabel. *Bull. Amer. Meteor. Soc.*, **85**, 151-153.

Kuo, H.-C., R.-T. Williams, and J.-H. Chen, 1999: A possible mechanism for the eye rotation of typhoon Herb. *J. Atmos. Sci.*, **56**, 1659-1673.

Laing, A. G., and J. M. Fritsch, 1993: Mesoscale convective complexes in Africa. *Mon. Wea. Rev.*, **121**, 2254-2263.

Laing, A. G., and J. M. Fritsch, 1997: The global population of mesoscale convective complexes. *Quart. J. Meteor. Soc.*, **123**, 389-405.

Laing, A. G., and J. M. Fritsch, 2000: The large-scale environments of the global populations of mesoscale convective complexes. *Mon. Wea. Rev.*, **128**, 2756-2776.

Lilly, D. K., 1979: The dynamical structure and evolution of thunderstorms and squall lines. *Ann. Rev. Earth Planet. Sci.*, **7**, 117-171.

Lin, Y.-L., K. E. Robertson, and C. M. Hill, 2005: Origin and propagation of a disturbance associated with an African easterly wave as a precursor of Hurricane Alberto (2000). *Mon. Wea. Rev.*, **133**, 3276-3298.

Lin, Y.-L., T.-A. Wang, and R. P. Weglarz, 1993: Interactions between gravity waves and cold air outflows in a stably stratified uniform flow. *J. Atmos. Sci.*, **50**, 3790-3816.

Ludlam, F. H., 1963: Severe local storms: a review. *Meteor. Monogr.*, **5**, Amer. Meteor. Soc., 1-30.

Madden, R. A., and P. R. Julian 1994: Observations of the 40-50 day tropical oscillation – A review. *Mon. Wea. Rev.*, **122**, 814-837.

Maddox, R. A., 1980: Mesoscale convective complexes. *Bull. Amer. Meteor. Soc.*, **61**, 1374-1387.

Maddox, R. A., 1983: Large-scale meteorological conditions associated with midlatitude mesoscale convective complexes. *Mon. Wea. Rev.*, **111**, 1475-1493.

Maddox, R. A., K. W. Howard, D. L. Bartels, and D. M. Rodgers, 1986: Mesoscale convective complexes in the middle latitudes. In *Mesoscale Meteorology and Forecasting*, P. S. Ray (Ed.), Amer. Meteor. Soc., 390-413.

Marks, F. D., Jr., and R. A. Houze, Jr., 1987: Inner-core structure of Hurricane Alicia from airborne Doppler-radar observations. *J. Atmos. Sci.*, **44**, 1296-1317.

McBride, J. L., 1995: Tropical cyclone formation. *Global Perspectives on Tropical Cyclones*. R. Elsberry, Ed., WMO No. TCP-38, 63-105.

Merrill, R. T., 1988: Characteristics of the upper-tropospheric environmental flow around hurricanes. *J. Atmos. Sci.*, **45**, 1665-1677.

Miller, D., and J. M. Fritsch, 1991: Mesoscale convective complexes in the western Pacific region. *Mon. Wea. Rev.*, **119**, 2978-2992.

Molinari, J., and D. Vollaro, 2000: Planetary- and synoptic-scale influence on eastern Pacific tropical cyclogenesis. *Mon. Wea. Rev.*, **128**, 3296-3307.

Moncrieff, M. W., 1978: The dynamical structure of two-dimensional steady convection in constant vertical shear. *Quart. J. Roy. Meteor. Soc.*, **104**, 543-567.

Montgomery, M. T., and B. F. Farrell, 1992: Polar low dynamics. *J. Atmos. Sci.*, **49**, 2484-2505.

Montgomery, M. T., and B. F. Farrell, 1993: Tropical Cyclone Formation. *J. Atmos. Sci.*, **50**, 285–310.
Neumann, C., 1993: Global overview. *Global Guide to Tropical Cyclone Forecasting WMO/TD-560*, G. J. Holland (Ed.), pp.3.1-3.46. World Meteor. Org., Geneva.
Newton, C. W., 1963: *Dynamics of severe convective storms*. *Meteor. Monogr.*, **5**, Amer. Meteor. Soc., 33-58.
Ogura, Y., and Y.-L. Chen, 1977: A life history of an intense mesoscale convective storm in Oklahoma. *J. Atmos. Sci.*, **34**, 1458-1476.
Olsson, P. O., and W. R. Cotton, 1997: Balanced and unbalanced circulations in a primitive equation simulation of a midlatitude MCC. Part II: Analysis of balance. *J. Atmos. Sci.*, **54**, 479-497.
Ooyama, K., 1964: A dynamical model for the study of tropical cyclone development. *Geophys. Int.*, **4**, 187-198.
Ooyama, K., 1969: Numerical simulation of the life cycle of tropical cyclones. *J. Atmos. Sci.*, **26**, 3-40.
Ooyama, K., 1982: Conceptual evolution of the theory and modeling of the tropical cyclone. *J. Meteor. Soc. Japan*, **60**, 369-380.
Palmén, E., 1948: On the formation and structure of tropical cyclones. *Geophysics*, **3**, 26-38.
Parker, M. D., and R. H. Johnson, 2000: Organization modes of midlatitude mesoscale convective systems. *Mon. Wea. Rev.*, **128**, 3413-3436.
Parker, M. D., and R. H. Johnson, 2004a: Structures and dynamics of quasi-2D mesoscale convective systems. *J. Atmos. Sci.*, **61**, 545-567.
Parker, M. D., and R. H. Johnson, 2004b: Simulated convective lines with leading precipitation. Part I: Governing dynamics. *J. Atmos. Sci.*, **61**, 1637-1655.
Persing, J., and M. T. Montgomery, 2003: Hurricane superintensity. J. Atmos. Sci., **60**, 2349-2371.
Rasmussen, E. R., 1979: The polar low as an extratropical CISK disturbance. *Quart. J. Roy. Meteor. Soc.*, **105**, 531-549.
Raymond, D. J., and H. Jiang, 1990: A theory for long-lived mesoscale convective systems. *J. Atmos. Sci.*, **47**, 3067-3077.
Redelsperger, J.-L., and T. L. Clark, 1989: The initiation and horizontal scale selection of convection over gently sloping terrain. *J. Atmos. Sci.*, **47**, 516–541.
Reed, R. J., 1979: Cyclogenesis in polar air streams. *Mon. Wea. Rev.*, **107**, 38-52.
Riehl, H., 1948: On the formation of typhoons. *J. Meteor.*, **5**, 247-264.
Riehl, H., 1954: T*ropical Meteorology*. McGraw-Hill Co., 392pp.
Ritchie, E. A., and G. J. Holland 1993: On the interaction of tropical-cyclone scale vortices. II: interacting vortex patches. *Quart. J. Roy. Meteor. Soc.*, **119**, 1363-1397.
Ritchie, E. A., and G. J. Holland, 1997: Scale Interactions during the Formation of Typhoon Irving. *Mon. Wea. Rev.*, **125**, 1377–1396.
Rotunno, R., and K. A. Emanuel, 1987: An air-sea interaction theory for tropical cyclones. Part II: Evolutionary study using a nonhydrostatic axiymmetric numerical model. *J. Atmos. Sci.*, **44**, 140-153.
Rotunno, R., J. B. Klemp, and M. L. Weisman, 1988: A theory for strong, long-lived squall lines. *J. Atmos. Sci.*, **45**, 463-485.
Schubert, W. H., J. J. Hack, P. L. Silva Dias, and S. R. Fulton, 1980: Geostrophic adjustment in an axisymmetric vortex. *J. Atmos. Sci.*, **37**, 1464-1484.

Schubert, W. H., M. T. Montgomery, R. K. Taft, T. A. Guinn, S. R. Fulton, J. P. Kossin, and J. P. Edwards, 1999: Polygonal eyewalls, asymmetric eye contraction, and potential vorticity mixing in hurricanes. *J. Atmos. Sci.*, **56**, 1197-1223.

Smith, R. K., 1980: Tropical cyclone eye dynamics. *J. Atmos. Sci.*, **37**, 1227-1232.

Smith, R. K., 1997: On the theory of CISK. *Quart. J. Roy. Meteor. Soc.*, **123**, 407-418.

Takeda, T., 1971: Numerical simulation of a precipitating convective cloud: The formation of a "long-lasting" cloud. J. Atmos. Sci., **28**, 350-376.

Thiao, W, R. A. Scofield, and J. Robinson, 1993: The relationship between water vapor plumes and extreme rainfall events during the summer season, *NOAA Technical Report*, *NESDIS*, **67**, 69 pp.

Tripoli, G. J., and W. R. Cotton, 1989: Numerical study of an observed orogenic mesoscale convective system. Part I: Simulated genesis and comparison with observations. *Mon. Wea. Rev.*, **117**, 273-304.

Wang, Y., 2002: Vortex Rossby waves in a numerically simulated tropical cyclone. Part I: Overall structure, potential vorticity, and kinetic energy budgets. *J. Atmos. Sci.*, **59**, 1213-1237.

Weisman, M. L., and R. Rotunno, 2004: "A theory for strong long-lived squall lines" revisited. *J. Atmos. Sci.*, **61**, 361-382.

Weisman, M. L., J. B. Klemp, and R. Rotunno, 1988: Structure and evolution of numerically simulated squall lines. *J. Atmos. Sci.*, **45**, 1990-2013.

Willoughby, H. E., 1998: Tropical cyclone eye thermodynamics. *Mon. Wea. Rev.*, **126**, 3053-3067.

Willoughby, H. E., F. D. Marks, and R. J. Feinberg, 1984: Stationary and moving convective bands in hurricanes. *J. Atmos. Sci.*, **41**, 3189-3211.

Wu, C.-C., and K. A. Emanuel, 1993: Interaction of a baroclinic vortex with background shear: application to hurricane movement. *J. Atmos. Sci.*, **50**, 62-76.

Wu, C.-C., and Kurihara, 1996: A numerical study of the feedback mechanisms of hurricane-environment interaction on hurricane movement from the potential vorticity perspective. *J. Atmos. Sci.*, **53**, 2264-2282.

Xu, Q., 1992: Density currents in shear flows - A two-fluid model. *J. Atmos. Sci.*, **49,** 511-524.

Xue, M., 2000: Density currents in two-layer shear flows. *Quart. J. Roy. Met. Soc.*, **126**, 1301-1320.

Zhang, D.-L., Y. Liu, and M. K. Yau, 2002: A multiscale numerical study of Hurricane Andrew (1992). Part V: Inner-core thermodynamics. *Mon. Wea. Rev.*, **130**, 2745-2763.

Zipser, E. J., 1977: Mesoscale and convective-scale downdrafts as distinct components of squall-line structure. *Mon. Wea. Rev.*, **105**, 1568-1589.